HOKKAIDO UNIVERSITY

Title	Control of Concentration Boundary Layer Development by Time-Varying Electromagnetic Force Imposition near Solid-Liquid Interface
Author(s)	XU, Guangye
Degree Grantor	北海道大学
Degree Name	博士(工学)
Dissertation Number	甲第15347号
Issue Date	2023-03-23
DOI	https://doi.org/10.14943/doctoral.k15347
Doc URL	https://hdl.handle.net/2115/89483
Type	doctoral thesis
File Information	XU_Guangye.pdf

Control of Concentration Boundary Layer Development by Time-Varying Electromagnetic Force Imposition near Solid-Liquid Interface

XU Guangye

Laboratory of Novel Processing

Division of Materials Science and Engineering

Graduate School of Engineering

CONTENTS

Abstract

For solid-liquid chemical reactions, the mass transfer in a concentration boundary layer formed near the solid-liquid interface is often the rate-determining step. The mass transfer in it depends on diffusion and convection. The former positively relates to the diffusion coefficient and the concentration gradient. The diffusion coefficient control is difficult because it is one of the physical properties. Increasing the concentration gradient is an effective way to enhance the mass transfer. Convection increases the concentration gradient because it decreases the concentration boundary layer thickness by introducing the liquid with the initial concentration from the bulk region to the adjacent region of the solid-liquid interface. Therefore, a flow excitation in the bulk region has been used as traditional methods to enhance the mass transfer.

By exciting the flow in the bulk region, a velocity boundary layer forms near the solid-liquid interface because the velocity at the solid-liquid interface should be 0. The concentration boundary layer is usually thinner than the velocity boundary layer. The flow in the concentration boundary layer must be weak and it reduces the efficiency of enhancing the mass transfer. Thus, a strong force imposition in the bulk region is required. This degrades product qualities. The involvement of slags into a liquid metal in a refining process of the metallurgical industry and the void formation in the deposition layer in an electroplating process of the surface treatment industry due to the strong force imposition have been reported.

A new method was proposed to avoid these problems, which directly excited the flow in the concentration boundary layer by imposing an electromagnetic force. Because the force is induced by superimposing an electrical current and a magnetic field, this method is a powerful candidate for enhancing the mass transfer in industrial processes, such as the refining process in the metallurgical industry and the electroplating process in the surface treatment industry.

This dissertation discusses the concentration boundary layer development by adopting the newly proposed method. The outline of this dissertation is as follows:

Chapter 1 gives the general introduction of this dissertation, including traditional methods of the solid-liquid chemical reaction enhancement, and the objectives of this dissertation. The objectives include: (1) To study the concentration boundary layer development in a plane above the whole solid-liquid interface under the electromagnetic force imposition; (2) To study the mechanism of the time-varying electromagnetic force imposition on suppressing the concentration boundary layer development; (3) To optimize the condition of the solid-liquid chemical reaction enhancement by controlling the operating parameters of the electromagnetic force.

The objective of chapter 2 is to investigate the concentration boundary layer development in a plane above the whole solid-liquid interface by evaluating the time-variation of the solute concentration. The concentration boundary layer was formed by dissolving a Cu anodic into a Cu^{2+} aqueous solution. The brightness of the liquid solution near the anode surface was recorded by a camera, and the Cu^{2+} concentration was evaluated by using the measured brightness based on the Lambert-Beer's law. The flow pattern was observed by using the tracer particles, and Cu^{2+} concentration time variation under the electromagnetic force imposition was discussed based on the observed flow pattern. By imposing only the current, the Cu^{2+} concentration increased with time, which indicates the development of the concentration boundary layer. By imposing the electromagnetic force without the time-varying component, the increase of the Cu^{2+} concentration was suppressed, because of the excitation of a macro-scale flow in the whole vessel. However, high Cu^{2+} concentration was observed near the side parts of the solid-liquid interface because of the formation of stagnant zones near the side parts. This means that flow development near the solid-liquid interface depends on the shape of the solid-liquid interface. Consequently, the electromagnetic force imposition could not suppress the concentration boundary layer development in some regions near the solid-liquid interface. In addition, the concentration boundary layer development was further suppressed by imposing the time-varying electromagnetic force, and the Cu^{2+} concentration uniformly distributed in the measurement plane. The reasons were the enhancement of the macro-scale flow development and the excitation of a micro-scale flow near the anode surface. The micro-scale flow introduces liquid with initial Cu^{2+} concentration from the bulk region to the side parts of the anode surface and decreases the stagnant zone near the side parts.

The objectives of chapter 3 are to investigate the mechanism of the time-varying electromagnetic force imposition on suppressing the concentration boundary layer development by studying the reason for the micro-scale flow excitation, and to optimize the condition of the solid-liquid chemical reaction enhancement by controlling the amplitude or the frequency of the time-varying electromagnetic force. The reason for the micro-scale flow excitation was considered as the non-uniform electromagnetic force distribution near the anode surface caused by the non-uniform Cu^{2+} concentration distribution and the positive relationship between the Cu^{2+} concentration and the electrical conductivity. By imposing the time-varying electromagnetic force, the micro-scale flow development was enhanced compared to that by imposing the electromagnetic force without the time-varying component. The possible reason was considered as the enhancement of the non-uniform Cu^{2+} concentration distribution. Decreasing the time-

varying electromagnetic force frequency or increasing the time-varying electromagnetic force amplitude further enhanced the micro-scale flow development. Because the liquid with initial Cu^{2+} concentration flowed from the bulk region to the vicinity of the anode surface due to the micro-scale flow, the further enhancement of the micro-scale flow development contributes to further enhancing the solid-liquid chemical reaction.

Chapter 4 is the general conclusions of this dissertation.

Overall, the results of this dissertation prove that the imposition of the time-varying electromagnetic force is a promising way to enhance the solid-liquid chemical reaction. Compared to that by imposing the electromagnetic force without the time-varying component, the flow development is enhanced in both the macro-scale and the micro-scale. In addition, the flow can be controlled by controlling operating parameters. Therefore, the control of concentration boundary layer development by controlling operating parameters of the time-varying electromagnetic force is expected.

Chapter 1 General Introduction

1.1 Rate determining step of solid-liquid chemical reaction

The enhancement of the solid-liquid chemical reaction is important to promote energy and time saving. A solid-liquid chemical reaction system consists of the following steps [1-1]: (1) Diffusion of liquid reactants to the vicinity of the solid surface, (2) adsorption of the liquid reactants at the solid surface, (3) chemical reaction of the liquid reactants with the solid surface and (4) diffusion of the reaction products away from the reaction surface. If any one of the above steps is much slower than the others, that step becomes the rate-determining step. In other words, the rate-determining step for a solid-liquid chemical reaction in industrial processes is the chemical reaction rate or the mass transfer in a concentration boundary layer formed near the solid-liquid interface due to chemical species motion. For industrial processes with high solid-liquid chemical reaction temperatures, the chemical reaction rate increases with temperature, and mass transfer is often the rate-determining step, like a refining process in the metallurgical industry [1-2]. On the other hand, for industrial processes with a room chemical reaction temperature, the reactant supply by mass transfer is often the rate-determining step. For instance, an electroplating process in the surface treatment industry [1-3, 1-4]. The reactant concentration profile in the liquid phase near the solid-liquid interface is shown in Fig. 1.1 [1-1, 1-6]. Here, c_b is the reactant concentration in bulk liquid, c_l indicates the reactant concentration in the

concentration boundary layer, c_s is the reactant concentration at the solid surface, and y_1 indicates the concentration boundary layer thickness.
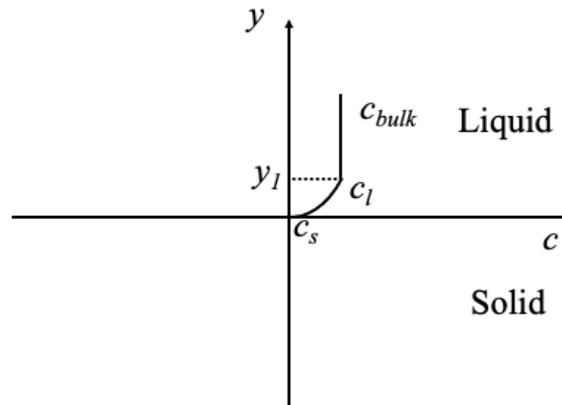

Fig. 1.1 Schematic diagram of reactant concentration profile near solid-liquid interface [1-1,1-6].

1.2 Traditional methods for solid-liquid chemical reaction enhancement

As mentioned in section 1.1, the mass transfer in the concentration boundary layer formed near the solid-liquid interface is often the rate-determining step for solid-liquid chemical reactions. The mass transfer in it depends on diffusion and convection [1-1,1-4,1-6]. The former one is described by Fick's first law [1-7]. Its intensity depends on the diffusion coefficient and the concentration gradient. However, the diffusion coefficient control is difficult because it is one of the physical properties. Therefore, increasing the concentration gradient near the solid-liquid interface is effective for enhancing the solid-liquid chemical reaction. Because the convection contributes to decreasing the

concentration boundary layer thickness by inducing the liquid with initial concentration from the bulk region to the adjacent region of the solid-liquid interface, it increases the concentration gradient near the solid-liquid interface. Thus, the force imposition in the bulk region for the excitation of flow has been used for enhancing solid-liquid chemical reactions [1-1,1-9 – 1-11].

1.2.1 Mechanical agitation method

The mechanical agitation method has been used in the refining process for the metallurgical industry and the electroplating process for the surface treatment industry as shown in Fig. 1.2 [1-12, 1-13]. By rotating the impeller in the bulk region of the liquid, a flow in the bulk region is excited.
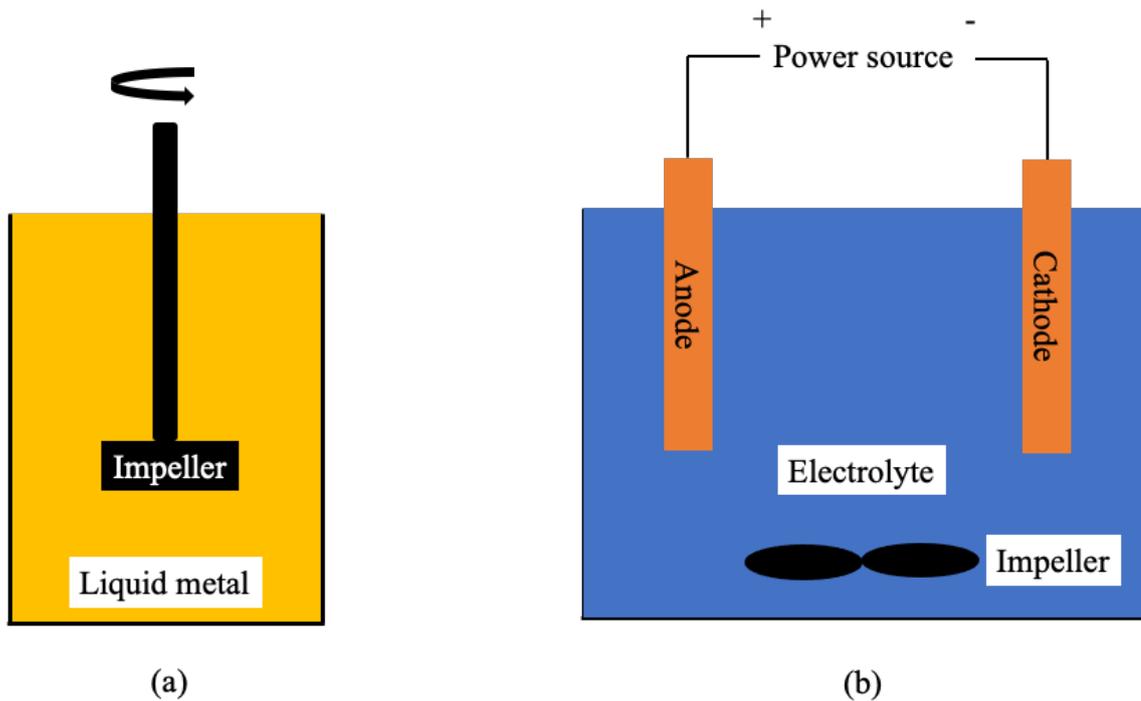
Fig. 1.2 Schematic diagrams of mechanical agitation method in (a) high-temperature

process [1-12] and (b) electroplating process [1-13].

Song et.al investigated the effect of the mechanical agitation on the mass transfer

by dissolving solid sodium thiosulphate into a starch-iodine aqueous solution at the room

temperature [1-14]. They found that the mechanical agitation method enhanced the mass

transfer because of the flow excitation. Kato et.al numerically simulated the flow pattern

and the mass transfer under the imposition of the mechanical agitation in a high-

temperature refining process [1-15]. They found that by increasing the impeller rotation

speed, the region with high kinetic energy was enlarged. This further enhanced the mass

transfer. Similar results have also been found in the electroplating process at the room temperature [1-13]. These results indicate that the mechanical agitation method enhances the mass transfer. However, the pollution of the liquid phase caused by the wear or corrosion of the impeller is one of the problems of this method, which might degrade the quality of the products.

1.2.2 Gas injection method

The gas injection method is another method for the enhancement of the solid-liquid chemical reaction. This method is commonly used in the refining process of the steel-making industry [1-16]. In this method, a nozzle is set at the top or bottom of the vessel. The former is called the top blowing and the latter is named the bottom gas injection, as shown in Fig. 1.3. Gases such as argon, nitrogen, and oxygen are usually used for injection. By injecting the gas, bubbles are successively generated at the nozzle exit and move upward through the effect of the buoyancy force. By this means, flow can be excited in the bulk region of the liquid. It has been found that by this method, the mass transfer can be enhanced because of the flow excitation [1-17 - 1-21]. However, the pollution of the liquid due to the corrosion of the nozzle and the splashing of the liquid from the bulk due to the rising of the bubbles are the problems of this method needed to be solved [1-22].
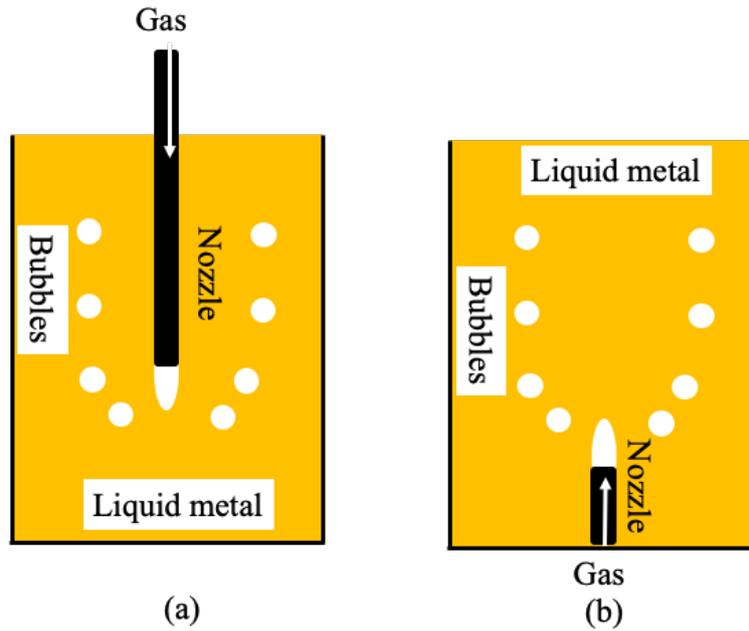
Fig. 1.3 Schematic diagrams of (a) top and (b) bottom gas injections [1-16].

1.2.3 Problems of traditional methods

By imposing the flow in the bulk region, a velocity boundary layer formed near the solid-liquid interface because the velocity of the liquid at the solid-liquid interface should be 0. The relative thickness between the velocity boundary layer and the concentration boundary layer is a function of the Schmidt number defined by the Eqs. (1.1) and (1.2) [1-8].

$$Sc = \frac{\nu}{D} \tag{1.1}$$

$$\frac{\delta_c}{\delta_v} = Sc^{-\frac{1}{3}} \tag{1.2}$$

Here D is the diffusion coefficient, ν is the kinematic viscosity, δ_c is the concentration

boundary layer thickness and δ_v is the velocity boundary layer thickness.
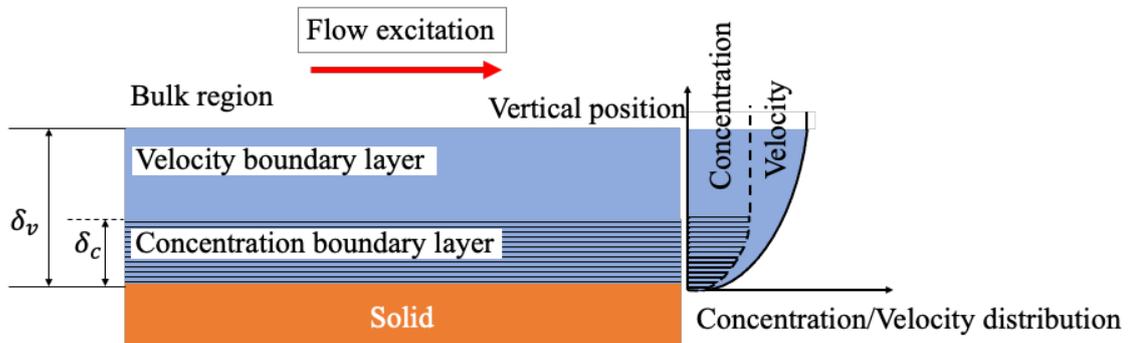

Fig. 1.4 Schematic diagram of concentration boundary layer, velocity boundary layer, and

concentration and velocity distributions in vertical direction from solid surface.

Because the Schmidt number is usually in the order of more than 100 for liquids [1-6],

the concentration boundary layer is in the inner part of the velocity boundary layer, as

shown in Fig. 1.4. The weak flow in the concentration boundary layer must reduce the

efficiency on decreasing the concentration boundary layer thickness in the traditional

methods. Thus, a strong force imposition in the bulk liquid is required [1-1]. The strong

force imposition degrades product qualities at the same time. The involvement of slags

into a liquid metal in the refining process and large voids formation in the deposition layer

fin the electroplating process have been reported [1-9, 1-13, 1-23].

1.3 Objective of this research

The principle and problems of the traditional methods have been introduced in section 1.2. The flow excitation in the bulk liquid does not effectively enhance the mass transfer. And a direct flow excitation in the concentration boundary layer is required. Based on this concept, a new method of exciting flow in the concentration boundary layer by imposing an electromagnetic force was proposed [1-1, 1-9, 1-23]. The electromagnetic force has been widely applied in industrial processes due to its' cleanliness and high controllability [1-24 – 1-32]. Because the flow is directly excited in the concentration boundary layer without physical contact, the problems in the traditional methods can be avoided. Based on this reason, the proposed method is a powerful candidate for enhancing the mass transfer in industrial processes such as the electroplating process in the surface treatment industry and the refining process in the metallurgical industry. For the electroplating process with current imposition, the excitation of the electromagnetic force by imposing the magnetic field is expected. On the other hand, the magnetic field and current have been widely used in high-temperature processes [1-33]. For instance, the magnetic field imposition in the continuous casting process and the current imposition in an electric arc furnace. Therefore, the adoption of the proposed method in the refining process of the metallurgical industry is also expected. In addition, because the electromagnetic force can be controlled by controlling the electrical current and the

magnetic field, the control of mass transfer is expected. The principle and merits of the

proposed methods are shown in Fig. 1.5.

Principle

Advection-diffusion equation

Convection Diffusion

$$\frac{\partial c}{\partial t} + (\boldsymbol{v} \cdot \nabla)c = D\nabla^2 c$$

Navier-stocks equation

$$\frac{\partial}{\partial t}\boldsymbol{v} + (\boldsymbol{v} \cdot \nabla)\boldsymbol{v} = -\frac{1}{\rho}\nabla p + \nu\nabla^2\boldsymbol{v} + \boldsymbol{F}$$

c: concentration D: diffusion coefficient ν : kinematic viscosity ρ : density

t: time v: velocity F: external force

Electromagnetic force

$$\boldsymbol{F} = J \times B$$

B: magnetic field F: electromagnetic force J: current density

Mass transfer is controllable by controlling convection;
By controlling the external force, the convection can be controlled;
By controlling the magnetic field and current, mass transfer can be controlled.

Merits

- Mass transfer can be controlled by controlling the magnetic field and current.

- Direct force imposition in the concentration boundary layer without physical contact.

- This method can be applied in industries dealing with a conductive liquid. e.g., the metallurgical industry and the aerospace industry.

Fig. 1.5 Principle and merit of newly proposed method [1-2, 1-34, 1-35].

Till now, the main method for evaluating the mass transfer intensity was the

calculation of the mass transfer coefficient or the measurement of the current density

under a constant voltage imposition [1-36 – 1-39]. Direct observations of the flow in the

concentration boundary layer and the concentration boundary layer development are

required. Based on this concept, the experimental works in this dissertation were conducted by using a visualizable Cu^{2+} aqueous solution model. Because of the inverse relationship between the Cu^{2+} concentration and the Cu^{2+} aqueous solution brightness according to the Lambert-Beer's law [1-40, 1-41], the development of the concentration boundary layer can be evaluated by measuring the liquid brightness near the solid-liquid interface.

Regarding the proposed method, Yokota et.al evaluated the concentration boundary layer development under the imposition of a direct current (DC current), the superimposition of a magnetic field with the DC current or a modulated current composed of the DC current and an alternating current (AC current) [1-40]. By superimposing the magnetic field with the DC current or the modulated current, an electromagnetic force without or with a time-varying component was excited. They found that the development of the concentration boundary layer was suppressed under the imposition of the electromagnetic force without the time-varying component compared to that with only the DC current imposition at a point above the solid-liquid interface. And by imposing the time-varying electromagnetic force, the concentration boundary layer development was further suppressed at the same position. However, because the solid-liquid interface in industrial processes is usually a plane, the result evaluated at one point is not enough

to optimize the condition for enhancing the solid-liquid chemical reaction, and the clarification of whether the concentration boundary layer development could be suppressed or not in a plane above the whole solid-liquid interface is required. Therefore, the objectives of this research were:

(1) To study the concentration boundary layer development in a plane above the whole solid-liquid interface under the imposition of the electromagnetic force.

(2) To study the mechanism of the time-varying electromagnetic force imposition on suppressing the concentration boundary layer development.

(3) To optimize the condition of the solid-liquid chemical reaction enhancement by controlling the operating parameters of the electromagnetic force.

1.4 Structure and contents of this dissertation

This dissertation includes the following chapters:

Chapter 1 introduces the principle of enhancing solid-liquid chemical reactions. The mass transfer is often the rate-determining step for solid-liquid chemical reactions, such as a refining process in the metallurgical industry and an electroplating process in the surface treatment process. To enhance the solid-liquid chemical reaction, the decrease of the concentration boundary layer thickness is an effective method. Therefore, traditional methods excite a flow in the bulk region of the liquid. However, because the concentration

boundary layer is thinner than the velocity boundary layer, flow in the concentration

boundary layer is limited in traditional methods. This means that the traditional methods

have limitation on enhancing mass transfer, and a strong agitation in the bulk liquid is

required. This degrades the product quality. A new method was proposed to avoid these

problems, which directly excited the flow in the concentration boundary layer by

imposing an electromagnetic force. The principle and merits of the proposed method were

described in this chapter. The results of the previous research regarding the proposed

method were also introduced in this chapter. The objectives of this dissertation were

introduced.

Chapter 2 aims to study the concentration boundary layer development in a plane above

the whole solid-liquid interface by evaluating the time variation of the solute

concentration under the imposition of a DC current or an electromagnetic force without

or with a time-varying component. The electromagnetic force without or with the time-

varying component was excited by superimposing a gradient magnetic field with a DC

current or a modulated current composed of the DC current and an AC current,

respectively. By imposing the DC current, the solute concentration increased with time,

because of the dissolution of the solid into the liquid. In addition, the non-uniform solute

concentration distribution with higher solute concentration near the side parts than that

near the middle part was observed, because of the current concentration near the side parts.

By imposing the electromagnetic force without the time-varying component, the increase

of the solute concentration was suppressed. This means that the concentration boundary

layer development was suppressed, because of the excitation of a macro-scale flow in the

whole vessel. The high solute concentration was observed near the side parts of the solid-

liquid interface. This was because of the formation of stagnant zones near the side parts

caused by the non-uniform electromagnetic force distribution. In addition, the

concentration boundary layer development was further suppressed by imposing the time-

varying electromagnetic force, and the solute concentration was uniformly distributed in

the measurement plane. These were because of the enhancement of the macro-scale flow

development and the excitation of a micro-scale flow near the solid-liquid interface.

Chapter 3 aims to investigate the mechanism of the time-varying electromagnetic force

imposition on suppressing the concentration boundary layer development by studying the

reason for the micro-scale flow excitation, and to optimize the condition of the solid-

liquid chemical reaction enhancement by controlling the operating parameters. The DC

current or the modulated current was superimposed with a uniform magnetic field. By

this means, the macro-scale flow excitation in the whole vessel was suppressed, and only

the micro-scale flow was excited in the vicinity of the solid-liquid interface. The non-

uniform distributed electromagnetic force and friction of side walls resulted in a higher solute concentration around the center than that close to the side walls in the front-to-back direction near one side part of the solid-liquid interface. Because of the positive relationship between the solute concentration and the electrical conductivity, the current concentration took place around the center. Therefore, the electromagnetic force component parallel to the solid-liquid interface around the center was larger than that close to the side walls. This force difference was the driving force for the micro-scale flow excitation. By imposing the time-varying electromagnetic force, the driving force for the micro-scale flow excitation was enhanced compared to that by imposing the electromagnetic force without the time-varying component. The decrease of the time-varying electromagnetic force frequency or the increase of its amplitude further enhanced the micro-scale flow excitation.

Chapter 4 summarized the results of this dissertation.

References

[1-1] C. Wen: *J. Ind. Eng. Chem.*, **60**(1968), 24.

[1-2] K. Iwai, T. Yokota, A. Maruyama and T. Yamada: *IOP Conf. Ser.: Mater. Sci. Eng.*, **424**(2018), 012051.

[1-3] F. Walsh: *Trans. IMF.*, **70**(1992), 95.

[1-4] P. Olivas, A. Alemany and F. Bark: *J. Appl. Electrochem.*, **34**(2004), 19.

[1-5] J. Madden and I. Hunter: *Microelectromech. Sys.*, **5**(1996), 24.

[1-6] M. Kosaka and S. Minowa: *Tetsu-to-Hagane*, **53**(1967), 983.

[1-7] M. Iguchi and O. Ilegbusi: Basic Transport Phenomena in Materials Engineering, 1st ed., Springer, Tokyo, (2014), 141.

[1-8] R. Bird, W. Stewart and E. Lightfoot: Transport Phenomena, 2nd ed., John Wiley & Sons, Inc., New York, (2007), 621.

[1-9] T. Yokota, A. Maruyama and K. Iwai: *Tetsu-to-Hagane*, **102**(2016), 119.

[1-10] E. Ramasetti, V. Visuri, P. Sulasalmi, T. Fabritius, J. Savolainen, M. Li and L. Shao: *Metals*, **9**(2019), 829.

[1-11] E. Ramasetti, V. Visure, P. Sulasalmi, T. Fabritius, J. Savolainen, M. Li and L. Shao: *Metals*, **9**(2019), 1048.

[1-12] J. Joshi, A. Oandit, and M. Sharma: *Chem. Engng. Sci.*, **37**(1982), 813.

[1-13] Y. Zhang, G. Dong, H. Wang and P. Cheng: *J. Electrochem. Soc.*, **162**(2015), D427.

[1-14] L. Song, M. Jolly, M. Kimata, W. Bujalske and A. Nienow: Third International Conference on CFD in the Minerals and Process Industries, CSRIO, Melbourne, (2003), 10.

[1-15] K. Kato, T. Yamamoto, S. Komarov, R. Taniguchi and Y. Ishiwata: *Mater. Trans.,* **60**(2019), 2008.

[1-16] T. Akiyama, M. Iguchi, K. Kurokawa, K. Matsuura, T. Mohri, S. Ohnuki, H. Takahashi and S. Ukai: Frontiers of Materials Science, IOS Press, Tokyo, (2007), 173-176.

[1-17] F. Richardson, D. Robertson, and B. Staples: Physical Chemistry in Metallurgy: The Darken Conference, U. S. Steel, Pittsburgh, (1976), 25.

[1-18] K. Nakanishi, Y. Kato, T. Nozaki and T. Emi: *Tetsu-to-Hagane*, **66**(1980), 1307.

[1-19] J. Ishida, K. Yamaguchi, S. Sugiura, K. Yamano, S. Hayakawa and N. Demukai: *Denki-Seiko*, **52**(1981), 2.

[1-20] B. Berg, G. Carlsson and M. Bramming: *Scand. J. Met*., **14**(1985), 299.

[1-21] A. Conejo: *Processes*, **8**(2020), 750.

[1-22] H. Kasahara and S. Taniguchi: *Teion Kogaku*, **43**(2008), 2.

[1-23] T. Yokota, A. Maruyama, T. Yamada and K. Iwai: *J. Japan. Inst. Met. Mater.*, **81**(2017), 516.

[1-24] S. Asai: Sci. *Technol. Adv. Mater.*, **4**(2000), 191.

[1-25] S. Asai: Magnetohydrodynamics, Springer, Dordrecht, (2007), 315.

[1-26] T. Fahidy: *Prog. Surf. Sci.*, **68**(2001), 155.

[1-27] J. Coey and G. Hinds: *J. Alloys. Compd.*, **326**(2001), 238.

[1-28] M. Uhlemann, H. Schlorb, J. Msellak and J. Chopart: *J. Electrochem. Soc.*, **151**(2004), C598.

[1-29] A. Krause, C. Hamann, M. Uhlemann, A. Gebert and L. Schultz: *J. Magn. Magn. Mater.*, **290-291**(2005), 261.

[1-30] S. Bodea, R. Ballou and P. Molho: *Phys. Rev.*, **69**(2004), 021605.

[1-31] V. Heresanu, R. Ballou and P. Molho: *J. Magn. Magn. Mater.*, **226-230**(2001), 1978.

[1-32] K. Msellak, J. Chopart, O. Jbara, O. Aaboubi and J. Amblard: *J. Magn. Magn. Mater.*, **281**(2004), 295.

[1-33] H. Kasahara and S. Taniguchi: *J. Cryo. Soc. Japan.*, **43**(2008), 2-6.

[1-34] E. Shvydkiy, E. Baake and D. Koppen: *Metals*, **10**(2020), 532.

[1-35] W. Zhu, S. Yu, C. Chen, L. Shi, S. Xu, S. Shuai, T. Hu, H. Liao, J. Wang and Z.

Ren: *Metals*, **11**(2021), 1846.

[1-36] L. Allam, F. Lazar, B. Benfedda and J. Chopart: *J. Solid. State. Electrochem.*, **25**(2021), 2041-2053.

[1-37] A. Olivier, J. Chopart, J. Douglade and C. Gabrielli: *J. Electroanal. Chem.*, **217**(1987), 443-452.

[1-38] S. Mori, M. Kumita, M. Takeuchi and A. Tanimoto: *J. Chem. Eng. Japan.*, **29**(1996), 229-243.

[1-39] S. Mori, K. Satoh and A. Tanimoto: *Electrochim. Acta.*, **39**(1994), 2789.

[1-40] D. Swinehart: *J. Chem. Educ.*, **39**(1962), 333.

[1-41] T. Mayerhöfer, H. Mutschke and J. Popp: *ChemPhysChem.*, **17**(2016), 1948.

Chapter 2 Concentration Boundary Layer Development under Time-Varying Electromagnetic Force Imposition

2.1 Introduction

For solid-liquid chemical reactions, mass transfer is often the rate-determining step [2-1, 2-2]. For instance, a refining process in the metallurgical industry and an electroplating process in the surface treatment industry. The mass transfer depends on diffusion and convection. The former is described by the Fick's first law, and its intensity depends on the diffusion coefficient and the concentration gradient. The diffusion coefficient control is difficult because it is one of the physical properties. Therefore, increasing the concentration gradient near the solid-liquid interface is effective to enhance mass transfer. Because convection decreases the concentration boundary layer thickness by introducing the liquid with initial concentration from the bulk region to the adjacent region of the solid-liquid interface, it increases the concentration gradient near the solid-liquid interface [2-3, 2-4]. Thus, a flow excitation in the bulk region has been used as the traditional method to enhance mass transfer [2-5 – 2-9].

By exciting the flow in the bulk region, a velocity boundary layer forms near the solid-liquid interface [2-10, 2-11]. Its relative thickness to the concentration boundary layer is a function of the Schmidt number [2-12]. Because the Schmidt number is much larger than unity for liquids, the concentration boundary layer exists in the velocity boundary layer. The weak flow in the concentration boundary layer indicates that the efficiency of

decreasing the concentration boundary layer thickness in the traditional method is limited, and a strong convection in the bulk liquid is required for the mass transfer enhancement. This also results in the degradation of product qualities at the same time. The involvement of slags into a liquid metal for the refining process in metallurgy and the formation of large voids in the deposition layer for the electroplating process have been reported [2-13, 2-14]. Therefore, flow excitation in the bulk liquid does not effectively enhance the mass transfer. A direct flow excitation in the concentration boundary layer is required for the concentration boundary layer thickness decrease. Based on this concept, a new method was proposed, which imposed a force directly near the solid-liquid interface by imposing an electrical current and a magnetic field simultaneously [2-13]. By this way, flow can be directly excited in the concentration boundary layer, and the decrease of concentration boundary layer thickness and the enhancement of mass transfer are expected.

Since the flow is excited by superimposing the electrical current and the magnetic field, this method is expected to be applied to processes treating a conductive liquid, like a metal refining process and the electroplating process [2-15 – 2-18]. Furthermore, because the force can be controlled by controlling the current and the magnetic field, flow control in the concentration boundary layer is expected [2-19 – 2-21].

In the previous study [2-13], Yokota et.al evaluated a Cu^{2+} concentration boundary layer

development by dissolving a Cu anodic electrode into a Cu^{2+} electrolyte aqueous solution just above the middle part of the anode surface. An electromagnetic force, without or with a time-varying component was excited by superimposing a DC current and a gradient magnetic field without or with an AC current. The results found that by imposing the electromagnetic force without the time-varying component, the concentration boundary layer development was suppressed compared to that with only the current imposition. And by imposing the time-varying electromagnetic force, the concentration boundary layer development was further suppressed. However, because the solid-liquid interface in industrial processes is usually a plane, the result evaluated at one point is not enough to optimize the condition for enhancing the solid-liquid chemical reaction, and the clarification of whether the concentration boundary layer development could be suppressed or not in a plane above the whole anode interface is required. To investigate this, similar experimental conditions to the previous research were adopted. That is, the electromagnetic force without or with the time-varying component was excited by imposing the gradient magnetic field and the DC current without or with an AC current. In this study, the concentration boundary layer development in a plane above the whole anode interface is required was evaluated, and the liquid flow pattern was observed to clarify the mechanism of the change in concentration boundary layer development by

imposing the electromagnetic force with or without the time-varying component.

2.2 Experimental method

Figure 2.1(a) indicates the longitudinal cross-section of the experimental apparatus. A transparent acrylic vessel with a 20 mm inner length, 4 mm inner depth and 10 mm height was filled with 0.3 mol/L $CuSO_4$ + 0.1 mol/L H_2SO_4 aqueous solution. Two parallel Cu electrodes were set in the upper and lower parts of the vessel. The upper one was cathode and the lower one was anode. The left and right sides of the lower Cu electrode were covered by 5 mm length insulators with a height of 180 μm. The coordinate system in this investigation was also defined in Fig. 2.1. The center of the anode surface in the horizontal direction was set as the axis origin, and the horizontal, vertical and anteroposterior directions were indicated as the x-axis. y-axis, and z-axis respectively. Fig. 2.1(b) shows the side view of the relative position between the vessel and the electromagnet. The vessel was set between the north pole (N pole) and the south pole (S pole) of an electromagnet. The distance between the center of the vessel in the z-direction and each pole was 75 mm. The N pole and the S pole were on the back side and the front side of the vessel, respectively.
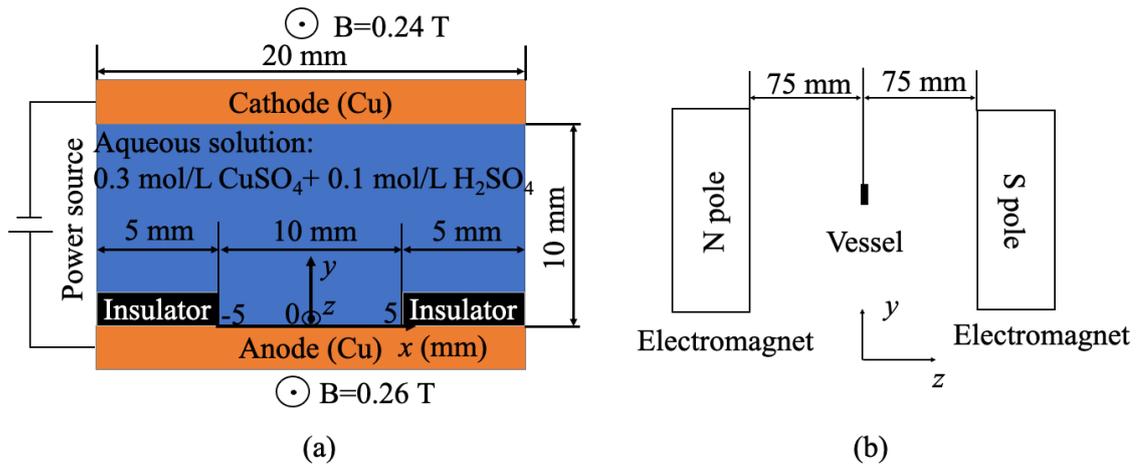
Fig. 2.1 (a) Longitudinal cross-section of experimental apparatus and (b) side view of

relative position between vessel and electromagnet.

The three experimental conditions are listed in Table 2.1 with their abbreviations.

The two current conditions were adapted. One was a 15 mA DC current, and the other

was a modulate current composed of a 15 mA DC current and a 2 Hz, 30 mAp-p AC

current, with the maximum and minimum intensities of 30 mA and 0 mA respectively.

These current conditions were the same to that adopted in the previous research [2-13]. The

average current intensities of these two conditions were 15 mA, and the average current

densities were 375 A/m^2 near the anode surface. In industrial applications, the current

densities are usually in the range of 100-300 A/m^2 [2-22]. Because the liquid motion in this

study was observed by using polystyrene tracer particles, as will be mentioned later, the

particle motion caused by the density difference between the aqueous solution and the

tracer particles might lead to the experimental error if the time for flow excitation is long. To accelerate the flow excitation, the current density adopted in this study was larger than that in the industrial application. Only the 15 mA DC current was imposed under the "DC condition", while a static horizontal gradient magnetic field perpendicular to the current direction as shown in Fig. 2.1 was superimposed with the DC current or the modulated current composed of the DC current and an AC current. Because the magnetic field intensity adopted in industrial applications is usually around 0.3 T, like in a continuous casting process of the steel-making industry [2-23], the magnetic field intensities near the anode and the cathode in this study were chosen around 0.3 T, with their intensities near the anode and near the cathodes were 0.26 T and 0.24 T, respectively. The experimental condition with superimposing the gradient magnetic field with the DC current or the modulated current was called the "DC+MF condition" or the "DC+AC+MF condition", respectively. Thus, the electromagnetic force without or with a time-varying component acted on the solution in the positive x-direction under the DC+MF condition and the DC+AC+MF condition, respectively. Because the intensity of the magnetic field near the anode was stronger than that near the cathode, the excitation of a counterclockwise circulating macro-scale flow is expected under the DC+MF and the DC+AC+MF conditions.

Table 2.1 Experimental conditions

	Experimental condition	DC current intensity (mA)	AC current intensity (mAp-p)	Magnetic field intensity near anode (T)	Magnetic field intensity near cathode (T)	Force condition
1	DC condition	15	0	0	0	no force
2	DC+MF condition	15	0	0.26	0.24	without time-varying component
3	DC+AC+MF condition	15	30	0.26	0.24	time-varying force

By imposing the electrical current, a Cu^{2+} concentration boundary layer forms near the solid-liquid interface since the solid Cu anode dissolves as Cu^{2+} into the aqueous solution. Based on the Lambert-Beer's law, the brightness of the aqueous solution used in this investigation depends on the Cu^{2+} concentration. Therefore, the Cu^{2+} concentration can be evaluated by measuring the liquid brightness based on the following equation [2-24, 2-25].

$$c = \frac{\log_{10}\left(\frac{I_1}{I_2}\right)}{-\epsilon l} + A \qquad (2.1)$$

where A is a constant, c is the Cu^{2+} concentration, I_1 is the brightness of objective liquid, I_2 is the brightness of a standard liquid, l is the light passing length in the absorbing

medium, and ϵ is the extinction coefficient, respectively.

By using this relation, the Cu^{2+} concentration was evaluated 200 μm above the anode (y=200 μm). A flat light source was set at the back of the vessel for uniform light incident. To exclude the error caused by the natural light, the experiments were conducted in a dark curtain. The brightness of the aqueous solution was recorded by a video recorder from the front side of the vessel with a frame rate of 50 frames per second and a pixel size of 40 μm×40 μm. Two prisms were set in the front side and the back side of the vessel. By this means, the concentration boundary layer development can be recorded from the front side of the vessel. However, by using the prisms, the recorded vessel was the reversal of the actual vessel in the horizontal direction. Because the vessel shape was symmetric, vessel reversal might not result in the experimental error on the concentration boundary layer development observation. The setup of the boundary layer observation system is shown in Fig. 2.2.
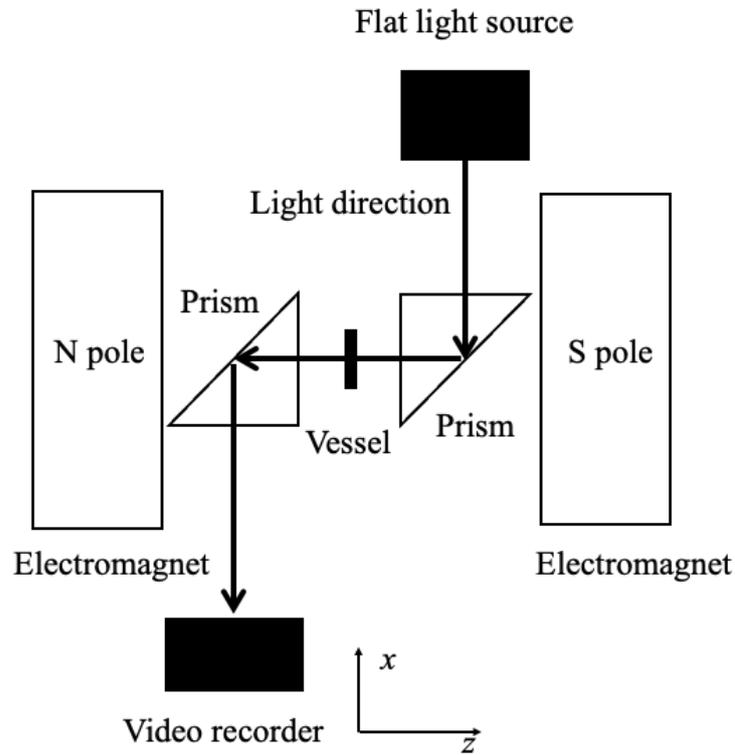
Fig. 2.2 Top view of concentration boundary layer development and liquid flow pattern

observation systems.

The liquid velocity was evaluated by using polystyrene tracer particles with a diameter

of 80 μm. The x-direction velocity was evaluated in the vertical y range of 160-240 μm.

For the expression convenience, the measurement range is expressed as the vertical

position of y=200 μm, which is the average vertical position of the vertical range. The y-

direction motion of the tracer particle caused by the density difference between the tracer

particle and the aqueous solution resulted in the falling down of the tracer particles, which

displaced the tracer particles away from the measurement range and led to the

experimental error. The terminal velocity u of the tracer particles caused by the density difference can be calculated by the following equation [2-26, 2-27]:

$$u = \frac{d^2 \Delta \rho g}{18\eta} \qquad (2.2)$$

where d is the diameter of the tracer particle, g is the gravitational acceleration, $\Delta\rho$ is the density difference between the liquid and the tracer particle and η is the liquid viscosity, respectively.

Because the terminal velocity was calculated as 31 μm/s, the particle displacement time from the measurement range length of 80 μm was 2.6 seconds. Thus, the particle motion measuring time was less than 2.6 s in this experiment to avoid the particle displacement from the measurement range. The relative position between the light source, video recorder and the vessel were the same with that shown in Fig. 2.2.

2.3 Experimental results and discussions

2.3.1 Cu^{2+} concentration distribution

Time dependence of the Cu^{2+} concentration distributions at the y position of 200 μm under the DC condition, the DC+MF condition, and the DC+AC+MF condition are shown in Fig. 2.3. The initial concentration distributions show deviation around the initial value of 0.3 mol/L, which was caused by the light reflection on the uneven anode surface, though the flat light source was used in this experiment. However, the spatial distribution

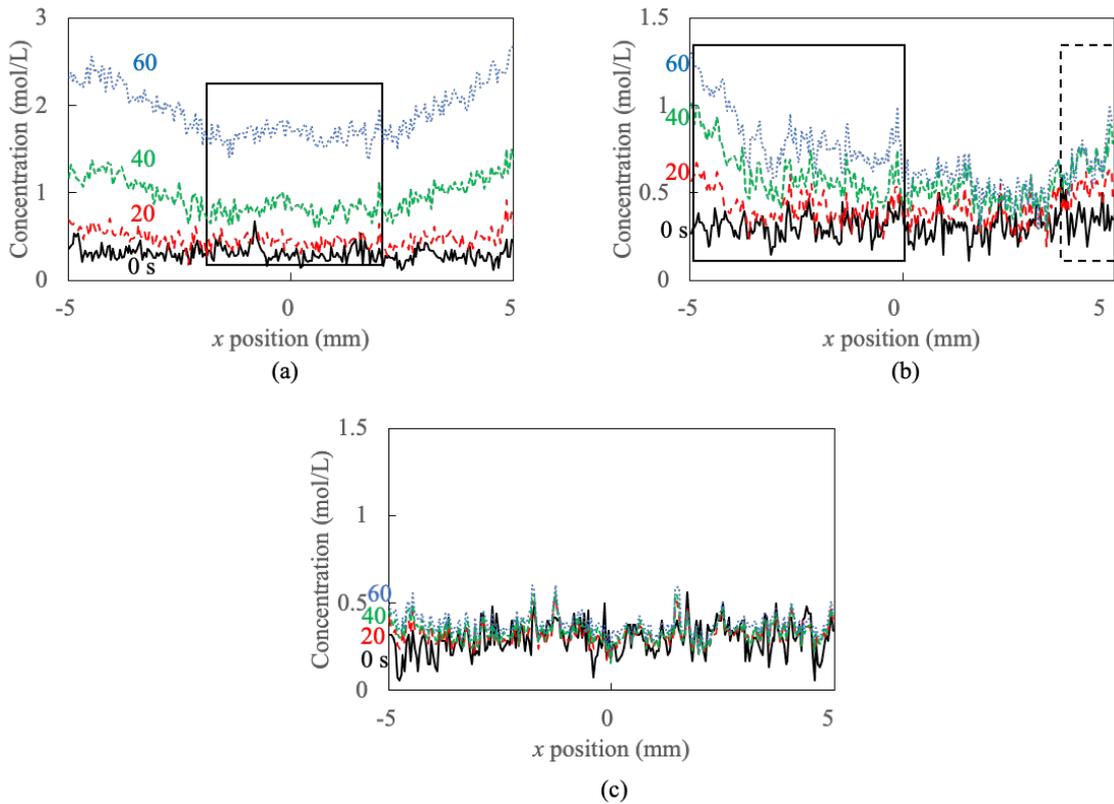and time dependence of the Cu^{2+} concentration can be evaluated because the deviation

was small.

Fig. 2.3 Time-dependence of Cu^{2+} concentration at 200 μm above anode under (a) DC

condition, (b) DC+MF condition and (c) DC+AC+MF condition.

An asymmetric Cu^{2+} concentration distribution was observed under the DC condition.

As shown in Fig. 2.3(a), near the middle part of the anode, where marked by the solid

square, the Cu^{2+} concentration was lower than that near the side parts of the anode. This

is caused by the current concentration near the side parts due to the length difference between the anode and the cathode [28]. Furthermore, as electrical conductivity of the aqueous solution has positive relation with the Cu^{2+} concentration [2-29, 2-30], the higher Cu^{2+} concentration near the side parts of the anode further enhanced the current concentration in these regions at the same time. Therefore, the Cu^{2+} concentration difference between near the side parts and near the middle part increased with time.

The uniform distribution of the Cu^{2+} concentration in the range of around -2 mm$<x<$2 mm near the middle part of the anode suggests that the uniform electrical current flowed perpendicular to the anode. In this x range, the Cu^{2+} concentrations at 0 s and 20 s were almost the same, whereas it increased obviously at 40 s and 60 s. This indicates that the Cu^{2+} diffusion distance at 20 s was less than 200 μm while it was close to 200 μm at 40 s and 60 s. On the other hand, the diffusion distance y can be estimated by the following equation in the case of one-dimensional diffusion phenomenon [2-31]:

$$y \sim \sqrt{D \cdot t_D} \qquad (2.3)$$

where D is diffusion coefficient and t_D is diffusion time, respectively.

Because the diffusion coefficient of Cu^{2+} ion in a 0.3 mol/L Cu^{2+} aqueous solution is about 5.5×10^{-10} m^2/s [2-32], the diffusion distance calculated using Eq. 2.3 is about 105 μm at 20 s, about 148 μm at 40 s and about 182 μm at 60 s. Thus, the observed results near

the middle part of the anode are in accordance with the theoretical evaluation results.

Figure 2.3(b) indicates the time dependence of the Cu^{2+} concentration distribution under the DC+MF condition. The asymmetrical Cu^{2+} concentration distribution with higher Cu^{2+} concentration near the side parts of the anode surface was observed, as marked by the solid square and the dashed square near the left and right parts respectively. The Cu^{2+} concentration obviously increased with time near the left part of the anode surface as marked by the solid square. In addition, a relative uniform Cu^{2+} concentration distribution was observed near the middle part of the anode surface.

Figure 2.3(c) shows the time dependence of the Cu^{2+} concentration distribution under the DC+AC+MF condition. Compared with that under the DC+MF condition, the Cu^{2+} concentration distributed more uniformly, and the increase of the Cu^{2+} concentration was suppressed. In addition, higher Cu^{2+} concentration near the side parts of the anode surface was not observed.
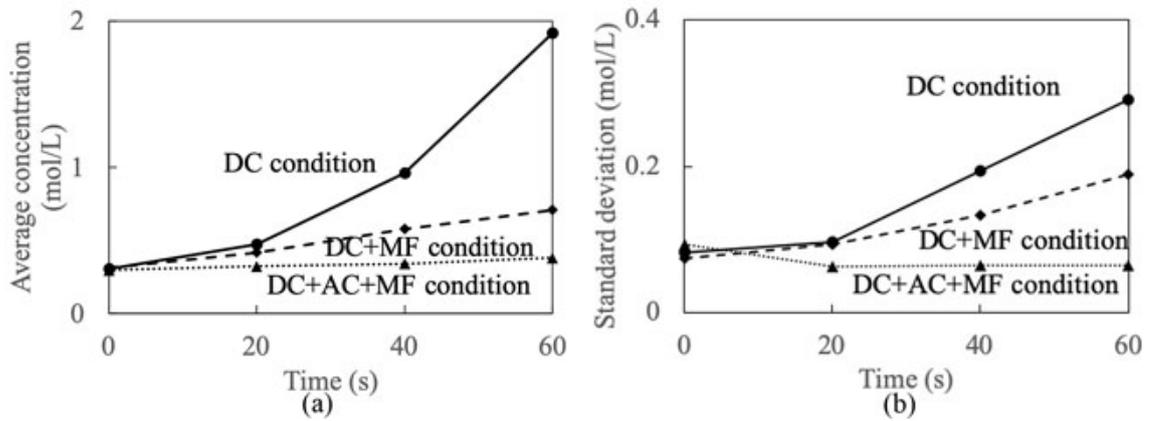
Fig. 2.4 (a) Average Cu^{2+} concentration and (b) standard deviation of Cu^{2+} concentration

distribution at 200 μm above anode.

Figure 2.4(a) shows the average Cu^{2+} concentration calculation results at the y

position of 200 μm under the DC condition, the DC+MF condition, and the DC+AC+MF

condition. The Cu^{2+} concentration increased with time under the DC condition, because

the dissolved Cu^{2+} from the anode gradually diffused towards the positive y direction. The

average concentration under the DC+MF condition was suppressed compared to that

under the DC condition. This means that the development of the concentration boundary

layer in the whole vicinity of the anode surface was suppressed by imposing the static

electromagnetic force compared to that without the force imposition. In contrast, no

obvious increase of the average Cu^{2+} concentration with time was observed under the

DC+AC+MF condition. Compared with that under the DC+MF condition, the average

Cu^{2+} concentration was further suppressed. This indicates a further suppression of the

concentration boundary layer development by imposing the time-varying electromagnetic force. Compared to the previous study [2-13], it was found that the suppression of the concentration boundary layer development by imposing the electromagnetic force without the time-varying force and its further suppression by imposing the time-varying electromagnetic force took place not only just above the center of the anode surface but also in the whole adjacent region of the anode surface.

The Cu^{2+} concentration distribution uniformity was evaluated by calculating the Cu^{2+} concentration distribution standard deviation at the y position of 200 μm, and the calculation results are shown in Fig. 2.4(b) under the three experimental conditions. Since these values under the three experimental conditions were almost the same at 0 s, the light reflection on the uneven anode surface did not affect the concentration uniformity evaluation results.

The standard deviation monotonically increased with time under the DC condition and the DC+MF condition. This is because the higher Cu^{2+} concentration near the side parts of the anode surface reduced the Cu^{2+} concentration distribution uniformity with time. In contrast, the standard deviation under the DC+AC+MF condition slightly decreased at 20 s, because the relatively dark solution by dissolving Cu^{2+} ion near the anode surface suppressed the light reflection caused by the uneven anode surface. Its

value was almost constant from 40 s to 60 s, because of the suppression of higher Cu^{2+}

concentration near the side parts of the anode surface. In addition, its magnitude was the

smallest among the three conditions. This means that the most uniform Cu^{2+} concentration

distribution in the concentration boundary layer was performed under the time-varying

electromagnetic force imposition.

2.3.2 Velocity measurement results

Figure 2.5 shows the electrical current flow curves and the electromagnetic force

directions under the DC+MF and the DC+AC+MF conditions. Near the middle part of

the anode surface, the current flowed perpendicular to the anode surface. However, near

the left and right parts, the current directions were not perpendicular to the anode surface

because of the length difference between the anode and the cathode [2-28], as indicated by

the dashed curves. Therefore, the directions of the excited electromagnetic forces near the

left, middle and right parts of the anode surface were oblique upward, parallel, and

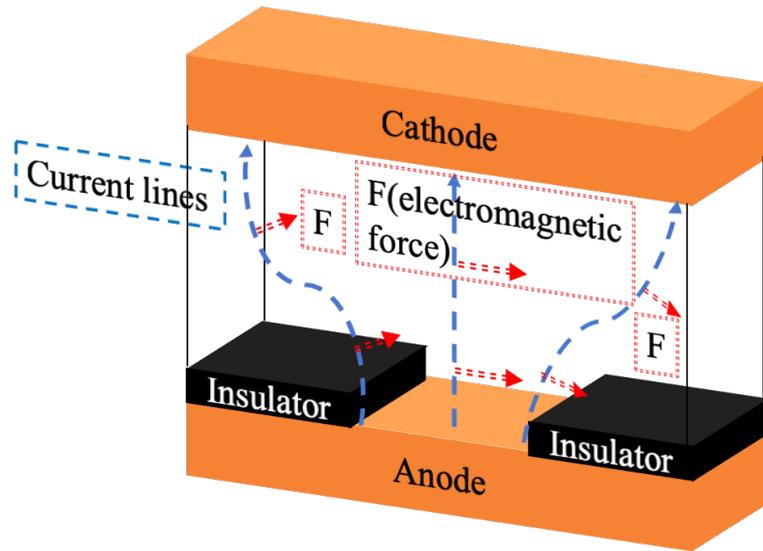oblique downward to the anode surface respectively, as marked by the dashed arrows.

Fig. 2.5 Schematic of electrical current flow curves and electromagnetic force directions

from 0 s to 60 s.

Figure 2.6 shows the liquid flow pattern under the DC+MF condition. A macro-scale flow was excited in the whole vessel within a few seconds, and its direction was counterclockwise from the front view. This is because of the 0.02 T magnetic field intensity difference between near the anode and near the cathode as has been shown in Fig. 2.1. Therefore, the liquid with initial 0.3 mol/L Cu^{2+} concentration flowed from the bulk region into the vicinity of the anode surface, and the development of the concentration boundary layer was suppressed compared to that under the DC condition as shown in Fig. 2.3(a).
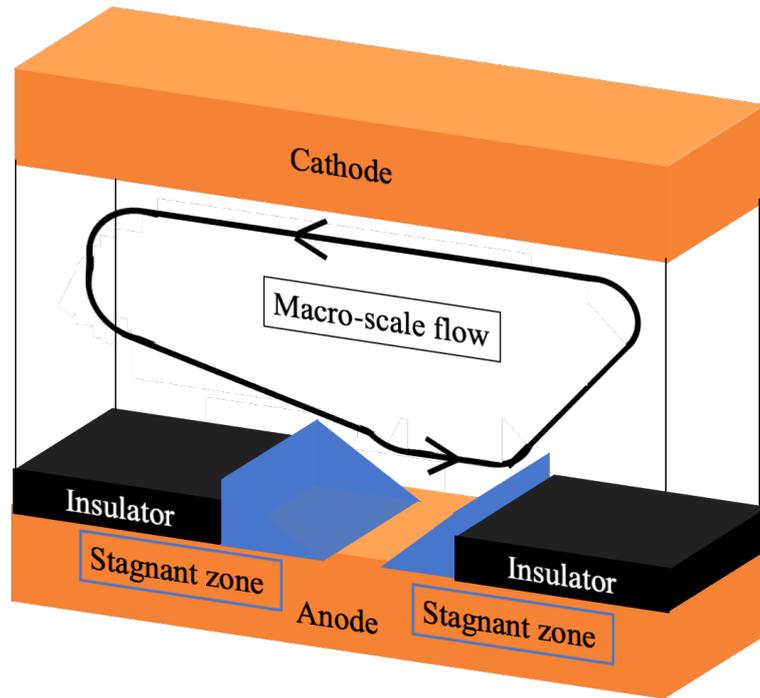
Fig. 2.6 Liquid flow pattern under DC+MF condition

An asymmetric macro-scale flow pattern was observed in the whole vessel as shown in Fig. 2.6, due to the asymmetric electromagnetic force direction distribution as shown in Fig. 2.5. Near the middle part of the anode surface, flow direction was parallel to the anode surface. This contributes to uniform the Cu^{2+} concentration distribution. Therefore, a relative uniform Cu^{2+} concentration distribution near the middle part was observed, as shown in Fig. 2.3(b). On the other hand, stagnant zones formed near the side parts of the anode surface. Noteworthy, the stagnant zone near the left part was larger than that near the right part. And the enlargement of the stagnant zone near the left part was observed. One of the reasons for the formation of the stagnant zones might be the 180 μm height

difference between the insulator and the anode [33]. An additional reason for that near the left part of the anode surface is considered as the oblique upward electromagnetic force as shown in Fig. 2.5. And near the right part, the upward component of the macro-scale flow according to the mass conservation law is supposed to be another reason for the formation of the stagnant zone. Because of the formation of the stagnant zones and the current concentration near the side parts, higher Cu^{2+} concentration was observed near the side parts as shown in Fig. 2.3(b). Since the electrical conductivity of the aqueous solution has positive relation with the Cu^{2+} concentration, the current concentration near the side parts was enhanced. This further enhanced the dissolution of the Cu^{2+} concentration from the left part of the anode. Furthermore, the electromagnetic force near the side parts increased. This might result in the enlargement of the stagnant zone near the left part, which also enhanced the increase of Cu^{2+} concentration near the left part. Therefore, Cu^{2+} concentration obviously increased with time near the left part compared to that near the middle and right parts, as shown in Fig. 2.3(b).

Figure 2.7 shows the maximum and minimum velocities at the y position of 200 μm under the DC+MF condition, which were evaluated by measuring the maximum and the minimum velocities of the tracer particles. Large velocity difference between the maximum and minimum velocity was observed. Because the liquid velocity at the side

walls of the vessel is 0, the velocity of the particles moving in the center of the vessel was larger than that moving close to the front or back walls of the vessel. This means that the maximum and the minimum velocities represent the characteristic velocities of the macro-scale flow in the center and close to the side walls of the vessel respectively. Thus, the minimum velocity was close to 0. On the other hand, the maximum velocity increased with time due to the development of the macro-scale flow. Because of the limitation of flow close to the side walls, a high Cu^{2+} concentration increase rate close to the side walls of the vessel compared to that in the center part in the z-direction is expected. As the Cu^{2+} concentration distribution evaluation results should be the average Cu^{2+} concentration in z-direction, a higher Cu^{2+} concentration increase rate close to the side walls of the vessel is supposed as a reason for the increase of the Cu^{2+} concentration under this condition as shown in Fig. 2.3(b).
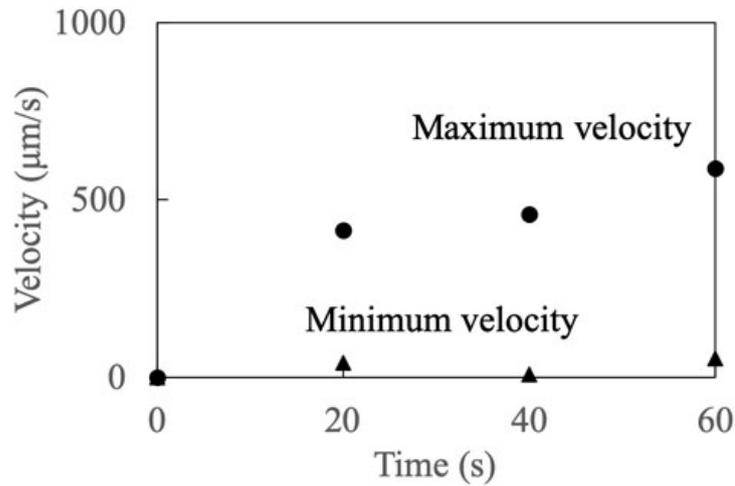
Fig. 2.7 Maximum and minimum velocities at y position of 200 μm under DC+MF

condition.

Figure 2.8 shows the serial change of the liquid flow pattern with time under the

DC+AC+MF condition. Similar to that under the DC+MF condition, the

counterclockwise asymmetric macro-scale flow was excited in the whole vessel within a

few seconds, because of the same average electromagnetic force distributions between

the DC+MF and the DC+AC+MF conditions. Furthermore, particle motions in the

positive and negative x-directions were simultaneously observed from about 5 s between

just above the insulator surface and the left and right parts of the anode surface. This

indicates that circulating micro-scale flows were excited from about 5 s as shown in Fig.

2.8(a). These flows were expressed as "anode-insulator micro-scale flows" in this

research. Besides, the liquid flow pattern changed with time. The liquid flow pattern

around 50-60 s is shown in Fig. 2.8(b). The anode-insulator micro-scale flow near the right part of the vessel shrank and was only observed above the right side insulator surface. However, no obvious shrinkage of the anode-insulator micro-scale flow was observed near the left part. In addition, another micro-scale flow was excited just above the right part of the anode surface at around 50 s. This flow was expressed as "local micro-scale flow" in this research. The excitation of the micro-scale flows indicates that the liquid flow pattern changed, and a local flow was excited in the vicinity of the solid-liquid interface by imposing the time-varying electromagnetic force compared to that under the imposition of the static electromagnetic force.
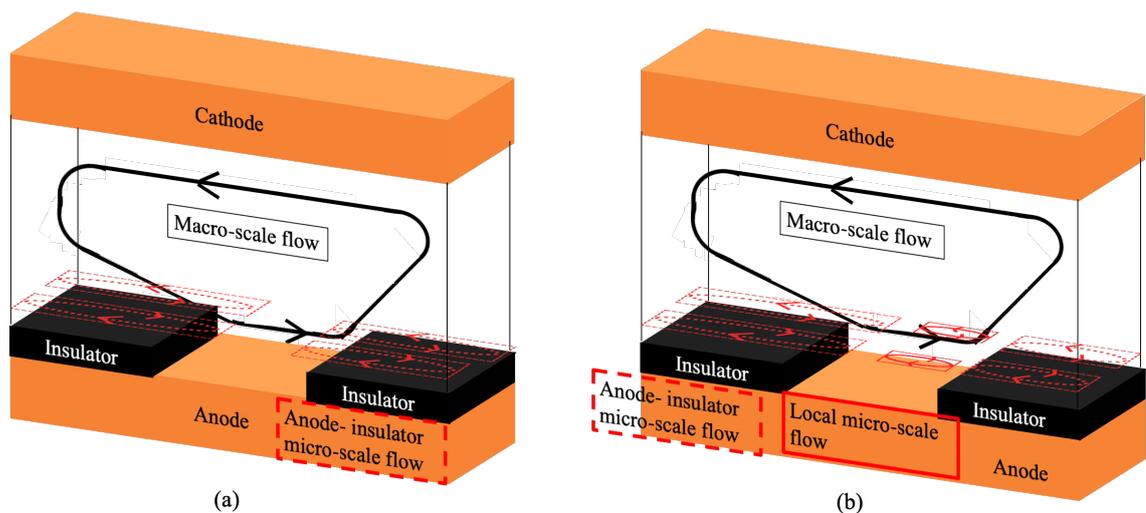

Fig. 2.8 Liquid flow pattern under DC+AC+MF condition around (a) 5- 50 s and (b) 50- 60 s.

The macro-scale flow contributes to uniform the Cu^{2+} concentration distribution especially near the middle part of the anode surface. On the other hand, because of the excitation of the anode-insulator micro-scale flows near the side parts of the anode surface, the liquid with initial 0.3 mol/L Cu^{2+} concentration flowed from just above the left and right part of the insulators to the left and right parts of the anode surface. This suppressed the increase of the Cu^{2+} concentration near the side parts and uniformed the Cu^{2+} concentration distribution. Besides, the local micro-scale flow also contributes to uniform the Cu^{2+} concentration distribution by mixing the liquid with higher Cu^{2+} concentration with the liquid with lower Cu^{2+} concentration. Owing to the excitation of the micro-scale flows, the higher Cu^{2+} concentration near the side parts was not observed, and the Cu^{2+} concentration distributed more uniformly compared to that under the DC+MF condition, as shown in Fig. 2.3(c).

Figure 2.9 shows the maximum and minimum velocities at the y position of 200 μm under the DC+AC+MF condition. Due to the observation of the negative x-direction particle motion, the minimum velocity was the negative value. This means that the minimum velocity represents the characteristic velocity of the micro-scale flow (the anode-insulator micro-scale flow or the local micro-scale flow). The absolute value of the minimum velocity increased from 20 s to 40 s and slightly decreased from 40 s to 60 s.

On the other hand, because the maximum velocity shown in Fig. 2.9 was much larger than the absolute value of the minimum velocity, and the absolute values of the positive and negative velocity components of the micro-scale flow should be in the same magnitude, the maximum velocity represents the characteristic velocity of the macro-scale flow. The maximum velocity increased with time, owing to the development of the macro-scale flow. Its magnitudes at 20 s were about 1000 μm/s, which was much larger than that of about 400 μm/s under the DC+MF condition as shown in Fig. 2.7. In addition, the maximum velocity difference between 20 s and 60 s was about 100 μm/s, which is smaller than that of about 200 μm/s under the DC+MF condition. These mean that the development of the macro-scale flow was enhanced by imposing the AC current. The enhancement of the macro-scale flow development might be another reason for the suppression of the Cu^{2+} concentration boundary layer development compared to that under the DC+MF condition as shown in Fig. 2.3(c).
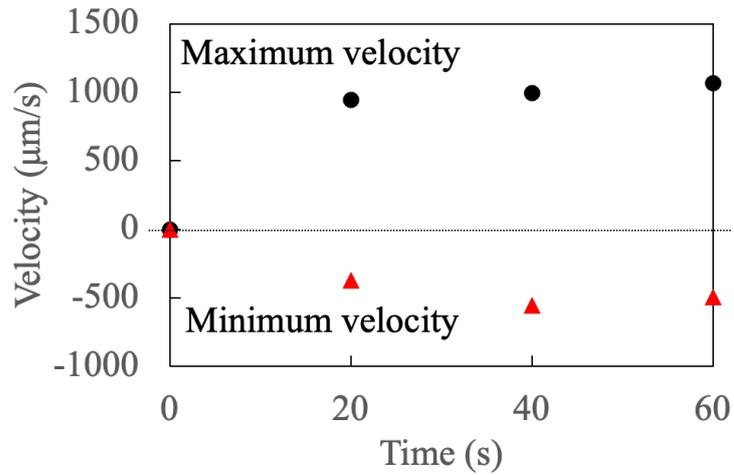
Fig. 2.9 Maximum and minimum velocities at *y* position of 200 μm under DC+AC+MF

condition.

2.4 Conclusions

To study the concentration boundary layer development in a plane above the solid-liquid interface under the imposition of the electromagnetic force, fundamental experiments were conducted. The following results can be achieved:

1. By imposing the electromagnetic force without the time-varying component, a macro-scale flow in the whole vessel was excited, which suppressed the concentration boundary layer development.

2. By imposing the time-varying electromagnetic force, the development of the concentration boundary layer was further suppressed compared to the imposing of the electromagnetic force without the time-varying component, and the solute

concentration distribution uniformity was enhanced.

3. The mechanism of the further suppression of the concentration boundary layer development by imposing the time-varying electromagnetic force was clarified. One of the reasons is the enhancement of the macro-scale flow in the whole vessel. The other is the excitation of a micro-scale flow in the vicinity of the solid-liquid interface. The micro-scale flow excitation homogenized the solute concentration distribution near the solid-liquid interface.

References

[2-1] M. Hirasawa, K. Mori, M. Sano, Y. Shimatani and Y. Okazaki: *Tetsu-to-Hagané*, **73** (1987), 1350.

[2-2] D. Landolt: *J. Electrochem. Soc.*, **149**(2002), S9.

[2-3] E. L. Cussler: Diffusion: Mass transfer in fluid systems, Cambridge university press, New York, (2009), 2.

[2-4] P. Atkins and J. D. Paula: Physical chemistry for the life sciences, Oxford University Press, New York, (2011), 219.

[2-5] N. Kohda: *Kaitei-Kinzokubutsurigakujoron*, CORONA PUBLISHING CO., LTD, Tokyo, (1973), 102.

[2-6] T. Sukawa and M. Iguchi: *Tetsu-to-Hagané*, **90** (2004), 334.

[2-7] K. Mori: *Tetsu-to-Hagané*, **77** (1991), 2077.

[2-8] T. Emi: *Tetsu-to-Hagané*, **100** (2014),31.

[2-9] M.Hirasawa, K. Mori, M. Sano, A. Hatanaka, Y. Shimatani and Y. Okazaki: *Tetsu-to-Hagané*, **73** (1987), 1343.

[2-10] R.F. Probstein: Physicochemical hydrodynamics: an introduction, John Wiley & Sons, New Jersey, (2005), 11.

[2-11] R. B. Bird: *Appl. Mech. Rev.*, **55** (2002), R1.

[2-12] T. L. Bergman, A. S. Lavine, F. P. Incropera and D. P. Dewitt: Fundamentals of heat and mass transfer, John Wiley & Sons, New Jersey, (2011), 378.

[2-13] T. Yokota, A. Maruyama, T. Yamada and K. Iwai: *J. Japan. Inst. Met. Mater*, **81** (2017), 516.

[2-14] Y. Zhang, G. Dong, H. Wang and P. Cheng: *J. Electrochem. Soc.*, **162** (2015), D427.

[2-15] C. Wang, Y. B. Zhong, J. Wang, Z. Q. Wang, W. L. Ren, Z. S. Lei and Z. M. Ren: *J. Electroanal. Chem.*, **630** (2009), 42.

[2-16] X. P. Li, Z. J. Zhao, H. L. Seet, W. M. Heng, T. B. Oh and J. Y. Lee: *J. Appl. Phys.*, **94** (2003), 6655.

[2-17] A. A. Tzavaras, and H. D. Brody: *JOM*, **36** (1984), 31.

[2-18] T. Weier, J. Hüller, G. Gerbeth, F. P. Weiss: *Chem. Eng. Sci.*, **60** (2005), 293.

[2-19] A. Bejan: Convection heat transfer, John Wiley & Sons, New Jersey, (2013), 2.

[2-20] R. F. Probstein: Physicochemical Hydrodynamics, John Wiley & Sons, New Jersey, (1994), 32.

[2-21] G. P. Galdi: An introduction to the mathematical theory of the Navier-Stokes equations: Steady-state problems, Springer Science & Business Media, Berlin, (2011), 14.

[2-22] H. Kasahara and S. Taniguchi: *J. Cryo. Soc. Japan.*, **43**(2008), 2-6.

[2-23] K. Fueki: Denkikagakubenran, 4th ed., Maruzen, (1985), 378-383.

[2-24] D. F. Swinehart: *J. Chem. Educ.*, **39** (1962), 333.

[2-25] T. G. Mayerhöfer, H. Mutschke, and J.Popp: *ChemPhysChem*,**17** (2016), 1948.

[2-26] S. Taniguchi and J. Yagi: Transport phenomena in materials engineering, Tohoku University Press, Sendai, (2001), 43.

[2-27] A. Riazi and U. Türker: *Comp. Part. Mech.*,**6** (2019), 427.

[2-28] N. Kanani: Electroplating: basic principles, processes and practice, Elsevier, Kidlington, (2004), 116.

[2-29] I. D. Zaytsev, and G. G. Aseyev: Properties of aqueous solutions of electrolytes, CRC press, Boca Raton, (1992), 655.

[2-30] M. Kamata and M. Paku: *J. Chem. Educ.,* **84** (2007), 674.

[2-31] P. Olivas, A. Alemany, and F. H. Bark: *J. Appl. Electrochem*., **34** (2004), 19.

[2-32] A. Emanuel and D. R. Olander: *J. Chem. Engng Data*, **8** (1963), 31.

[2-33] Meinhard T. Schobeiri: Fluid mechanics for engineers: a graduate textbook, Springer Science & Business Media, Berlin, (2010), 14.

Chapter 3 Local Flow Excitation near Solid-Liquid Interface under Superimposition of Uniform Magnetic Field and Electrical Current

3.1 Introduction

Chapter 2 studied the concentration boundary layer development in the whole vicinity of the anode surface under the electromagnetic force with or without the time-varying component. The results found that the time-varying electromagnetic force imposition suppressed the concentration boundary layer development compared to that by imposing the electromagnetic force without the time-varying component. The reasons were the enhancement of the macro-scale flow in the whole vessel and the excitation of the micro-scale flow near the anode surface by imposing the time-varying electromagnetic force.

However, the reason why the micro-scale flow was excited is still unknown. In addition, an optimization condition for enhancing the solid-liquid chemical reaction enhancement has not been found. Therefore, experimental work has been done for the clarification of the micro-scale flow excitation mechanism and for optimizing the condition for the solid-liquid chemical reaction enhancement in this chapter.

3.2 Experimental methods

Figure 3.1(a) shows the bird-eye view of the experimental apparatus. The experimental apparatus, the aqueous solution and the definition of the coordinate system adopted in this chapter were the same with those adopted in chapter 2.
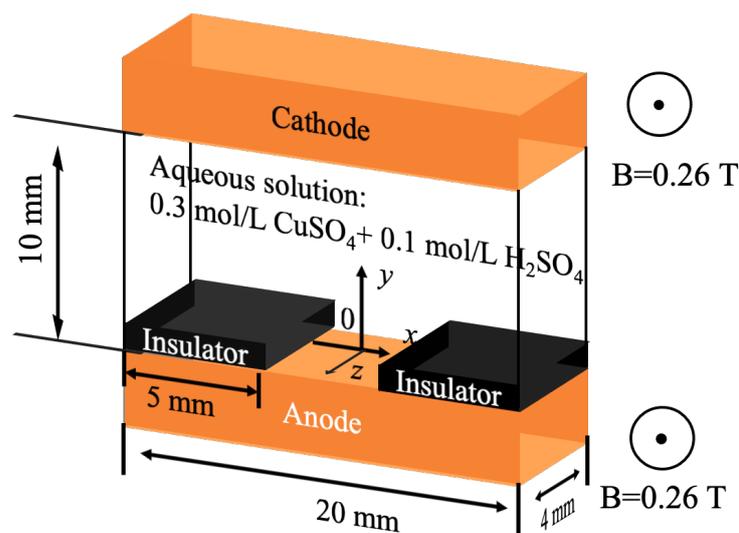
Fig. 3.1 Bird-eye view of experimental apparatus

The experimental conditions and their abbreviations are shown in Table 3.1. Four current conditions were adopted in this study. One was a 25 mA DC current. The others were modulated currents of the superimposition of the 25 mA DC current and a 2 Hz, 30 mAp-p AC current; the superimposition of the 25 mA DC current and a 6 Hz, 30 mAp-p AC current; and the superimposition of the 25 mA DC current and a 2 Hz, 50 mAp-p AC current. The average current intensities of these four current conditions were 25 mA. The experimental condition of only the 25 mA DC current imposition was expressed as the "DC condition". The experimental condition of the superimposition of the DC current and a uniform magnetic field was expressed as the "DC+MF condition". The experimental conditions of the simultaneous imposition of the uniform magnetic field and

the 2 Hz, 30 mAp-p, the 6 Hz, 30 mAp-p or the 2 Hz, 50 mAp-p modulated current were expressed as the "2 Hz, 30 mA condition", the "6 Hz, 30 mA condition", or the "2 Hz, 50 mA condition", respectively. The uniform magnetic field of 0.26 T was in the positive z-direction, and the magnetic field intensity near the anode was the same with those in chapters 2 and 3. The reason for adopting a uniform magnetic field in this chapter was to conduct the experiments without a macro-scale flow excitation. The magnetic field intensities near the anode and near the cathode were controlled by controlling the relative position between the vessel and the electromagnets in the vertical direction, while the relative position between the vessel and the electromagnets in the horizontal direction was the same with those shown in chapter 2, as shown in Fig. 2.1(b). Compared to those in chapter 2, the average current intensities in this study were intensified. This was to accelerate the micro-scale flow excitation.

Table 3.1 Experimental conditions

	Experimental condition abbreviation	DC current intensity (mA)	AC current amplitude (mA)	AC current frequency (Hz)	Magnetic field intensity near anode (T)	Magnetic field intensity near cathode (T)
1	DC condition	25	0	none	0	0
2	DC+MF condition	25	0	none	0.26	0.26
3	2 Hz, 30 mA condition	25	30	2	0.26	0.26
4	6 Hz, 30 mA condition	25	30	6	0.26	0.26
5	2 Hz, 50 mA condition	25	50	2	0.26	0.26

The Cu^{2+} concentration near the anode surface was evaluated by measuring the brightness near the anode surface [3-1 – 3-3]. The brightness measurement method was the same to that in chapter 2. Because the shape of the vessel was symmetric, the brightness was measured in the x-range of -1 mm to 5 mm and the y-range of 160 μm to 200 μm (one pixel in the vertical direction).

The liquid velocity was measured by using polystyrene particles with a diameter of 80 μm. The velocity measuring range was from -4 mm to 4 mm in the x-direction and 120 μm to 280 μm in the y-direction. The relative position between the light source, video recorder and the vessel were the same with those adopted in chapter 2, as shown in Fig.

2.2.

3.3 Experimental results and discussions

3.3.1 Concentration measurement results

Figure 3.2(a) shows the measured Cu^{2+} concentration distribution results under the DC condition. The average Cu^{2+} concentration in the x-ranges of -1 mm to 1 mm, 1 mm to 3 mm, and 3 mm to 5 mm was measured. For expression convenience, these x-ranges were named the x-positions of 0 mm, 2 mm, and 4 mm, respectively. The Cu^{2+} concentration increased with increasing the x-position. This corresponds to the previous results [3-3]. Because of the surface area difference between the cathode and the anode, the current concentration occurred near the right end of the anode surface [3-4]. That is, the current density near the right part was higher than that near the middle part. In addition, the concentration difference between 4 mm and 2 mm and between 4 mm and 0 mm increased with time. Because of the positive relationship between the electrical conductivity and the Cu^{2+} concentration [3-5, 3-6], the non-uniform current density distribution in the x-direction was enhanced. The Cu^{2+} concentration at 5 s was the minus value at 0 mm. The reason might be a slight irregular light reflection on the anode surface, even though the anode was polished. Figure 3.2(b) shows the comparison between the average Cu^{2+} concentration measurement results in the x-range of -1 mm to 5 mm and the

theoretical Cu^{2+} concentration under the DC condition. The theoretical Cu^{2+} concentration was calculated at the y-positions of 160 μm and 200 μm. For the theoretical Cu^{2+} concentration calculation, the diffusion phenomenon was simplified as a one-dimensional model in the positive y-direction. The boundary condition and the dissolved Cu^{2+} concentration near the anode surface when imposing a current from 0 s are shown in the following equations [3-7]:

$$c_{(y=0,t=0)} = c_0 \tag{3.1}$$

$$c_{(y=\infty,t=t)} = c_0 \tag{3.2}$$

$$2FD\left(\frac{\partial c}{\partial y}\right)_{y=0} = J \tag{3.3}$$

$$c_{y,t} - c_{y,0} = \frac{J}{2FD} \times \left[2\sqrt{\frac{Dt}{\pi}}\exp\left(-\frac{y^2}{4Dt}\right) - yerfc(\frac{y}{2\sqrt{Dt}})\right] \tag{3.4}$$

Here, c_0 is the initial concentration, $D=5.5 \times 10^{-10}$ m²/s [3-8, 3-9] is the Cu^{2+} diffusion coefficient, F is the Faraday's constant, J is the current density, t is the time, and y is the vertical position respectively.
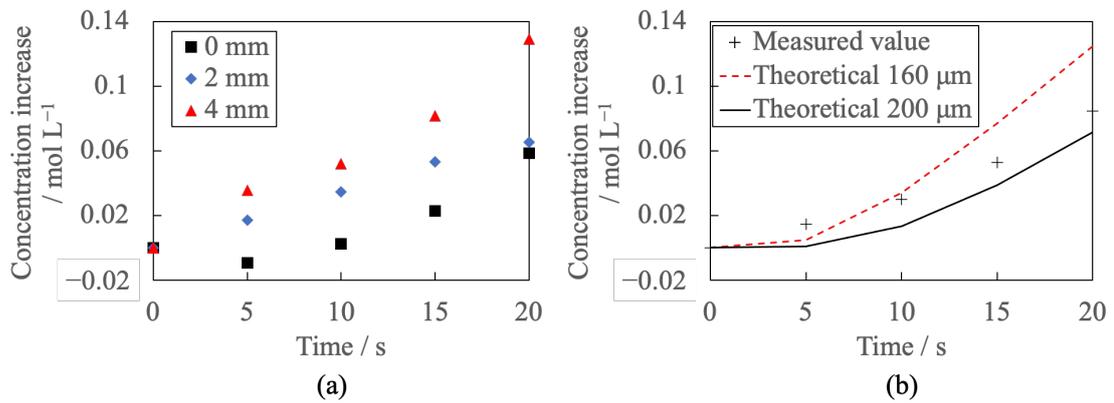
Fig. 3.2 (a) Concentration distribution and (b) comparison between theoretical Cu^{2+}

concentration at 160 μm, 200 μm and measured Cu^{2+} concentration under DC condition in *y*-

range of 160 μm - 200 μm.

The measured average concentration at 5 s was higher than the theoretical value at 160

μm and 200 μm. The reason might be the experimental error mentioned above. The

theoretical and measured concentrations agreed from 10 s to 20 s because the measured

average concentration was between the theoretical concentration calculation results at 160

μm and 200 μm. The concentration difference between the measured value and the

theoretical value at 160 μm increased, and the difference between the measured value and

the theoretical value at 200 μm decreased from 10 s to 20 s. This is attributed to the fact

that the Cu^{2+} concentration is inversely related to the Cu^{2+} diffusion coefficient [3-5, 3-6],

while the diffusion coefficient was constant in the theoretical calculation.

3.3.2 Velocity measurement results and liquid flow pattern observation results

A micro-scale flow was excited near the anode surface, and the macro-scale flow in the whole vessel was not excited except for the DC condition. Figure 3.3 shows the maximum velocity and the minimum velocity measurement results under the DC + MF condition. The maximum velocity and the absolute value of the minimum velocity were very close. Both of the velocities increased with time, while the increase rate became smaller. These indicate that the flow developed with time, and gradually approached the steady state.
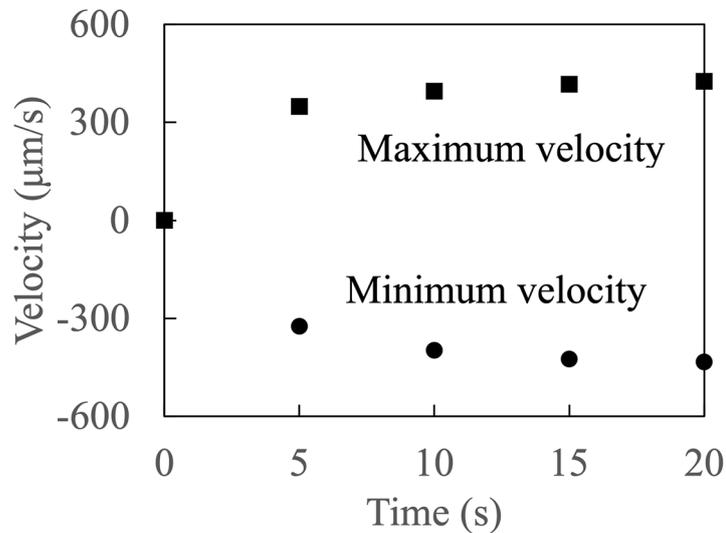

Fig. 3.3 Velocity measurement results under DC+MF condition in *x*-range of -4 mm to 4 mm and *y*-range of 120 μm to 280 μm.

Because the magnitudes of the two velocities were essentially the same under the

experimental conditions with the uniform magnetic field imposition, only the maximum velocity measurement results under these experimental conditions are shown in Figure 3.4. The maximum velocity under the experimental conditions with the modulated current imposition was larger than that under the DC+MF condition. This means that by superimposing the modulated current with the uniform magnetic field, the micro-scale flow excitation was enhanced compared to that under the DC+MF condition. Similar to that under the DC+MF condition, the flow gradually approached the steady state under the experimental conditions with the modulated current imposition. The higher maximum velocity under the 2 Hz, 30 mA condition compared to that under the 6 Hz, 30 mA condition indicates that by decreasing the modulated current frequency, the micro-scale flow excitation was enhanced. On the other hand, the maximum velocity under the 2 Hz, 50 mA condition was larger than that under the 2 Hz, 30 mA condition. This means that by increasing the modulated current amplitude, the micro-scale flow excitation was enhanced.
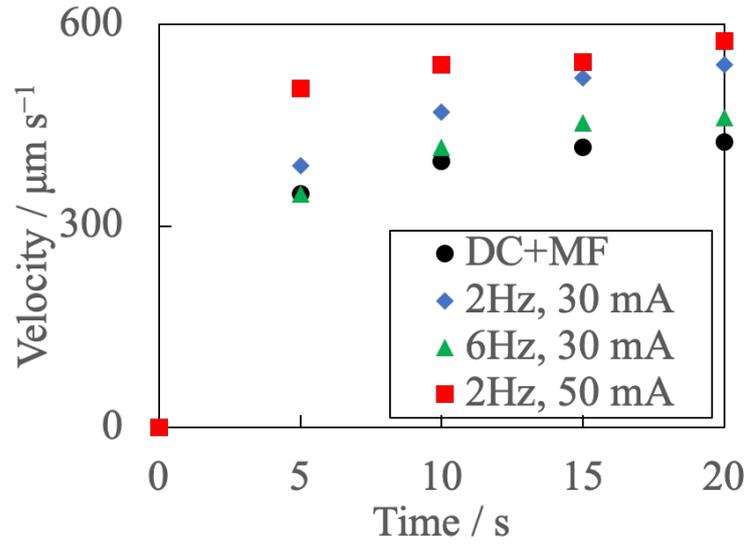
Fig. 3.4 Maximum velocity measurement results in x-range of -4 mm to 4 mm and y-range of

120 μm to 280 μm..

The liquid flow pattern under the DC+MF condition is shown in Fig. 3.5. The micro-

scale flow was essentially parallel to the anode surface and was observed just above the

anode surface. The flow in the center of the z-direction was in the positive x-direction,

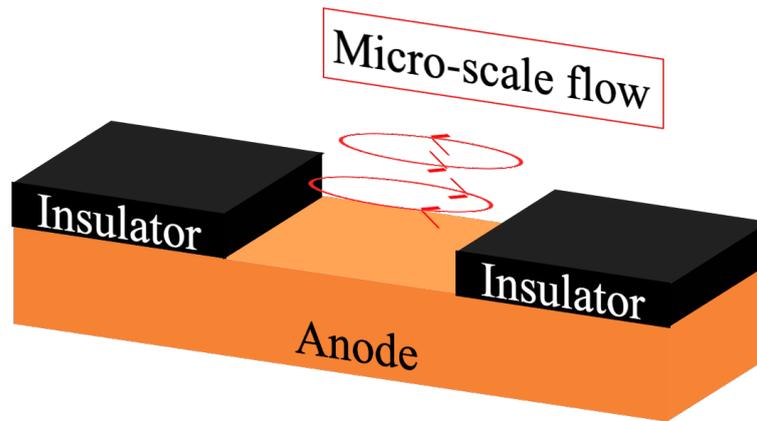while it was in the negative x-direction near the front and back walls.

Fig. 3.5 Liquid flow pattern under DC+MF condition from 5 s to 20 s in the *y*-range of 120

μm to 280 μm.

Figure 3.6 shows the liquid flow patterns under the 2 Hz, 30 mA condition and the 6

Hz, 30 mA condition. The liquid flow patterns under these two conditions were essentially

the same within 20 s, and the flow region expanded with time. The micro-scale flow was

observed above the anode surface at the initial stage, as shown in Figure 3.6(a). It first

expanded to above the upper part of the left-side insulator, as shown in Figure 3.6(b), and

it expanded to above the upper part of the right-side insulator at around 20 s, as shown in

Figure 3.6(c). The reason for the essentially same flow region under these two conditions,

while the maximum velocities were different might be the limitation of the experimental

time. The flow regions under these two conditions were larger than those under the

DC+MF condition shown in Figure 3.5. This corresponds to the results that the maximum

velocities under the 2 Hz, 30 mA condition and the 6 Hz, 30 mA condition were larger
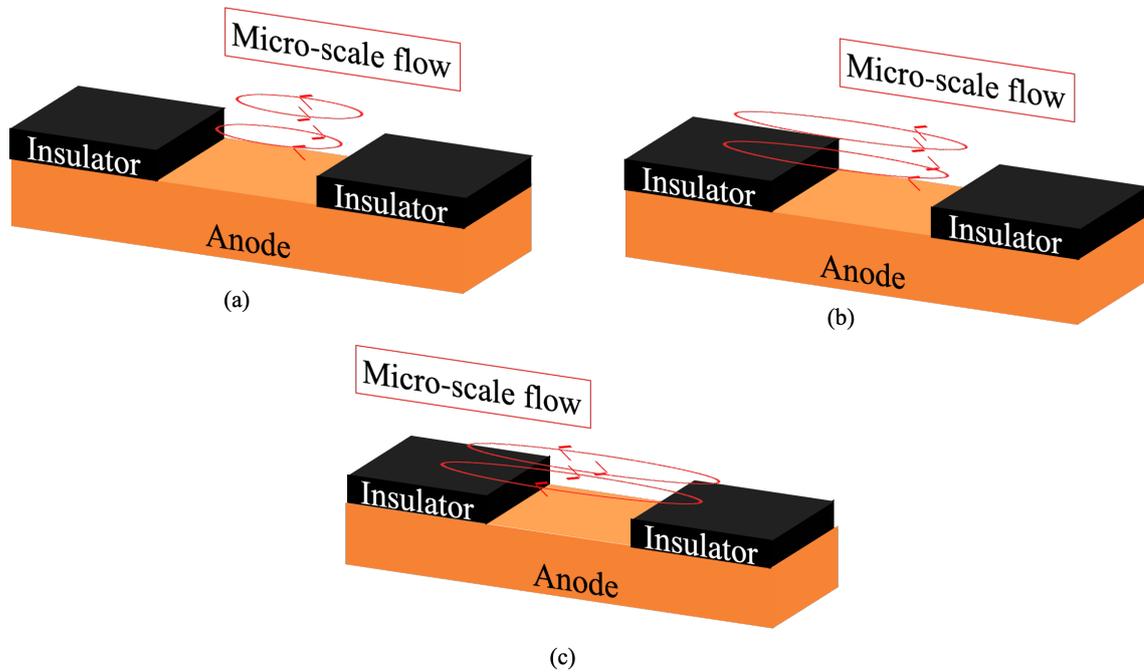
than those under the DC+MF condition.

Fig. 3.6 Liquid flow pattern under 2 Hz, 30 mA and 6 Hz, 30 mA conditions (a) at the initial

stage, and (b) and (c) with time development in the y-range of 120 μm to 280 μm.

The liquid flow pattern under the 2 Hz, 50 mA condition was different from those

under the DC+MF condition, the 2 Hz, 30 mA condition, and the 6 Hz, 30 mA condition,

as shown in Figure 3.7. The micro-scale flow was observed not only just above the anode

surface but also above the left and right sides' insulators from the initial stage. The largest

flow region under the 2 Hz, 50 mA condition corresponds to its largest maximum velocity

among all the experimental conditions with the uniform magnetic field imposition, as
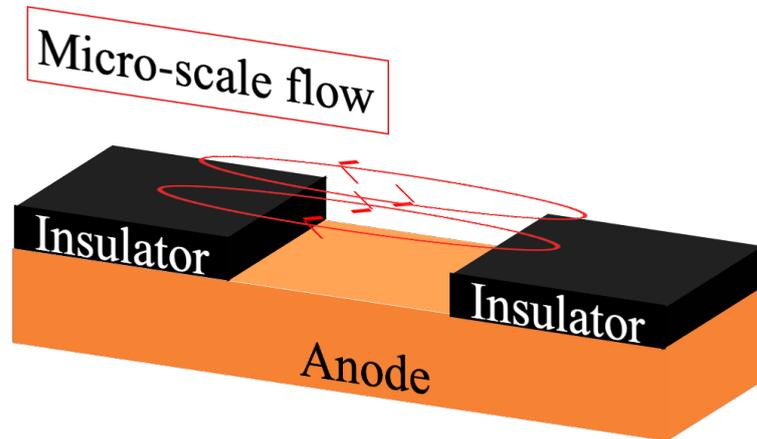
shown in Figure 3.4.

Fig. 3.7 Liquid flow pattern under 2 Hz, 50 mA condition from 5 s to 20 s in the *y*-range of

120 μm to 280 μm.

Figure 3.8 shows the mechanism of the micro-scale flow excitation. Because the

surface area of the cathode was two times larger than that of the anode, the current

concentration took place near the left and right parts of the anode's surface [3-4]. The

current directions near the left and right parts of the anode surface were not perpendicular

to the anode surface, as shown by the dashed arrows in Figure 3.8(a). Thus, the

electromagnetic force directions were oblique upward, parallel, and oblique downward to

the anode surface near the left, middle, and right parts, respectively. Near the left part of

the anode surface, the upward component of the electromagnetic force led to an upward

motion of liquid with a large Cu^{2+} concentration around the center in the z-direction

because the upward liquid motion near the front and back walls was suppressed due to

the friction, as shown in Figure 3.8(b). Therefore, the non-uniform Cu^{2+} concentration

distribution took place in the z-direction, in which the Cu^{2+} concentration near the front

and back walls was lower than that around the center in the z-direction, as shown in Figure

3.8(c). Because of the positive relationship between the Cu^{2+} concentration and the

electrical conductivity, the horizontal component of the electromagnetic force around the

center in the z-direction was larger than that near the front and back walls, as shown in

Figure 3.8(d), and this force difference increased with time. The electromagnetic force

difference in the z-direction was the driving force for the micro-scale flow excitation. The

time increase of this force difference was the reason for the development of the micro-

scale flow, as shown in Figure 3.4. Because of the larger horizontal component of the

electromagnetic force around the center in the z-direction, the micro-scale flow direction

around the center in the z-direction was the positive x-direction, and its direction near the

front and back walls was the negative x-direction, as shown in Figures 3.5-3.7. On the

other hand, because the micro-scale flow originated from the left part of the anode surface,

the flow region expanded towards the left at first, and then it expanded towards the right,

as shown in Figure 3.6.

During the large current half-period of the modulated current, the non-uniform Cu^{2+} concentration distribution in the z-direction, as shown in Figure 3.8(c), was enhanced under the experimental conditions with the modulated current imposition than that under the DC+MF condition. Furthermore, the positive relationship between the Cu^{2+} concentration and the electrical conductivity accelerated a further non-uniformity of the Cu^{2+} concentration distribution in the z-direction. During the small current half-period under the experimental conditions with the modulated current imposition, the larger Cu^{2+} concentration around the center in the z-direction remained because of the large electrical conductivity difference around the center and near the walls. Therefore, the driving force for the micro-scale flow excitation under the experimental conditions with the modulated current imposition was enhanced compared to that under the DC+MF condition. Thus, the expansion of the micro-scale flow region and the larger maximum velocity were observed under these experimental conditions in comparison with those under the DC+MF condition, even though the average current intensities were the same, as shown in Figures 3.4-3.7. The reason for the increase in modulated current frequency leading to the decrease in maximum velocity was not clarified. This will be investigated in future work. In addition, by increasing the modulated current amplitude, the driving force for the micro-scale flow excitation was further enhanced. Thus, the largest flow region and

the largest maximum velocity were observed under the 2 Hz, 50 mA condition from the initial stage among all the experimental conditions with the uniform magnetic field imposition.
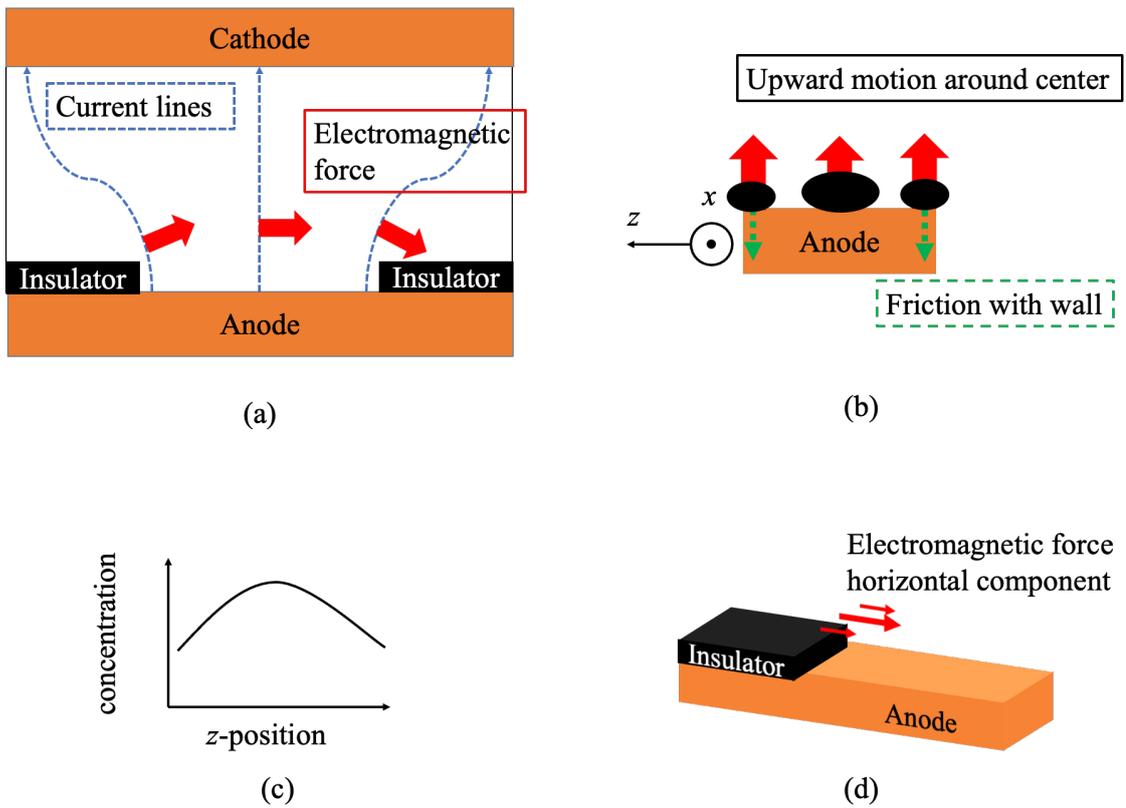

(a)

(b)

(c)

(d)

Fig. 3.8 Schematics of (a) current and electromagnetic force distributions, (b) right side view of upward liquid motion near the left side, (c) concentration distribution in z-direction and (d) electromagnetic force horizontal component distribution near left part.

3.4 Conclusions

To investigate the mechanism of a micro-scale flow excitation, the liquid flow pattern observation and its velocity measurement near the anode surface were conducted under the superimposition of a uniform magnetic field with a DC current or a modulated current. The following conclusions were obtained:

1. Only the micro-scale flow was observed near the anode surface under the experimental conditions with the current and the uniform magnetic field superimposition.

2. By superimposing the modulated current with the uniform magnetic field, the micro-scale flow excitation was enhanced compared to that under the superimposition of the DC current and the uniform magnetic field.

3. The decrease in modulated current frequency or the increase in modulated current amplitude enhanced the micro-scale flow excitation.

4. The mechanism of micro-scale flow excitation was clarified. That is, the driving force for the micro-scale flow excitation was the non-uniform electromagnetic force distribution in the z-direction caused by the non-uniform current distribution and the positive relationship between the Cu^{2+} concentration and the electrical conductivity.

References

[3-1] D. Swinehart: *J. Chem. Educ.*, **39**(1962), 333.

[3-2] T. Mayerhöfer, H. Mutschke, and J. Popp: *ChemPhysChem*, **17**(2016), 1948.

[3-3] G. Xu and K. Iwai: *ISIJ Int.*, **62**(2022), 1389.

[3-4] N. Kanani: Electroplating- Basic Principles, Processes and Practice, 1st ed., Elsevier, Amsterdam, (2005), 99-105.

[3-5] D. Price and W. Davenport: *Metall. Mater. Trans. B*, **11**(1980), 159.

[3-6] The Chemical Society of Japan: Handbook of Chemistry, Basics II, 3rd ed., Maruzen, Tokyo, (1984), 453.

[3-7] K. Fueki: Handbook of electrochemistry, 4th ed., Maruzen, Tokyo, (1985), 158.

[3-8] A. Emanuel and D. Olander: *J. Chem. Phys.*, **148**(2018), 134906.

[3-9] W. Eversole, H. Kindsvater and J. Peterson: *J. Phys. Chem.*, **3**(1942), 370.

Chapter 4 General Conclusions

To efficiently enhance the solid-liquid chemical reaction, a new method of direct flow excitation in the concentration boundary layer by imposing an electromagnetic force was proposed. The previous study regarding the proposed method found that the concentration boundary layer development was suppressed by imposing a time-varying electromagnetic force compared to that by imposing the electromagnetic force without the time-varying component at a point above the solid-liquid interface. However, because the solid-liquid interface in industrial processes is usually a plane, the result evaluated at one point is not enough to optimize the condition for enhancing the solid-liquid chemical reaction, and the clarification of whether the concentration boundary layer development could be suppressed or not in a plane above the whole solid-liquid interface is required. Therefore, the objectives of this research were:

(1) To study the concentration boundary layer development in a plane above the whole solid-liquid interface under the imposition of the electromagnetic force.

(2) To study the mechanism of the time-varying electromagnetic force on suppressing the concentration boundary layer development.

(3) To optimize the condition of the solid-liquid chemical reaction enhancement by controlling the operating parameters of the electromagnetic force.

The findings of this research are as follows:

Chapter 2 studied the concentration boundary layer development in a plane above the whole solid-liquid interface by evaluating the time variation of the solute concentration under the imposition of the electromagnetic force. The results found that by imposing the time-varying electromagnetic force, the concentration boundary layer development in the whole vicinity of the solid-liquid interface was suppressed compared to that by imposing the electromagnetic force without the time-varying component, and the solute concentration distribution was uniform. The reasons were that by imposing the time-varying electromagnetic force, the development of a macro-scale flow in the whole vessel was enhanced compared to that by imposing the electromagnetic force without the time-varying component, and a micro-scale flow was excited near the solid-liquid interface.

Chapter 3 investigated the mechanism of the time-varying electromagnetic force imposition on suppressing the concentration boundary layer development by studying the reason for the micro-scale flow excitation, and this chapter optimized the condition of the solid-liquid chemical reaction enhancement by controlling the frequency and the amplitude of the time-varying electromagnetic force. The reason for the micro-scale flow excitation was the non-uniform distributed electromagnetic force caused by the non-uniformed current distribution near the anode surface and the positive relationship between the solute concentration and the electrical conductivity. By superimposing the

modulated current with the uniform magnetic field, the micro-scale flow excitation was enhanced compared to that by superimposing the DC current with the uniform magnetic field. The decrease of the modulated current frequency or the increase of the modulated current amplitude further enhanced the micro-scale flow excitation.

In conclusion, this research found that the time-varying electromagnetic force imposition is useful for enhancing mass transfer. Compared to the traditional method of mass transfer enhancement by force imposition in the bulk region of a liquid, the force is directly imposed in the concentration boundary layer, which suppresses its development effectively. On the other hand, the time-varying electromagnetic force imposition enhanced the flow development compared to that by imposing the electromagnetic force without the time-varying component in both the macro-scale and the micro-scale flow. Furthermore, this research found that by controlling the frequency or the amplitude of the time-varying electromagnetic force, the flow pattern near the solid-liquid interface can be controlled. Therefore, the control of the concentration boundary layer development to optimize the condition of solid-liquid chemical reaction enhancement in industrial applications by controlling the time-varying electromagnetic force is expected.

Acknowledgements

I wish to express my great appreciation to everyone who have offered me invaluable help during the years for me studied at Hokkaido University.

First and foremost, I would like to express my sincere gratitude to my supervisor, Professor Kazuhiko IWAI, for his guidance, patience, and immense knowledge. His guidance helped me not only in my research, but also let me understand the meaning of an admirable human being. Besides my supervisor, I would like to thank Associate Professor Tatsuya OHMI and Associate Professor Qi ZHANG, for their kind guidance, useful ideas and comments on my research works. And I sincerely wish everything goes on well for their future life.

Secondly, I would like to appreciate Mr. Takumi OHHARA, Mr. Ko MAEDA, Mr. Masamune IWAHANA, Mr. Mao SHINO, Mr. Kiyokaze FUJITA, Mr. Tomosumi FUJIMURA, Mr. Tetsuya HASEGAWA, Ms. Rikako ISOZAKI, Mr. Tatsuru YOSHIDA, and Mr. Shuolei LI. For all the interesting time we had in the last year and valuable discussion we did during the seminar. Wish those who will continuous their research work in this laboratory could have nice academic achievements, and those who will start their new life as a society could have a bright future.

Thirdly, I am grateful to Mr. Yohei NISHI, Mr. Ginga KUSUNOKI, Mr. Shunpei

List of Research Accomplishments

Published manuscripts

(1) Guangye Xu, Kazuhiko Iwai: Solute Concentration Distribution in the Vicinity of Solid-Liquid Interface under the Imposition of a Time-Varying Force, ISIJ International, Vol. 62, No. 7, pp. 1389-1395 (2022). **(Chapter 2)**

(2) Guangye Xu, Kazuhiko Iwai: Micro-Scale Flow Excitation under Imposition of Uniform Magnetic Field and Electrical Current, Metals, Vol.12, No.12, pp 2034 (2022). **(Chapter 3)**

(3) Qi Zhang, Guangye Xu, Kazuhiko Iwai: Effective Removal Zone of Inclusions in a Horizontal Channel under A. C. Magnetic Field Imposition, ISIJ International, Vol. 61, No. 1, pp. 42-48 (2021).

(4) Qi Zhang, Guangye Xu, Kazuhiko Iwai: Effect of an AC Magnetic-field on the Dead-zone Range of Inclusions in the Circular Channel of an Induction-heating Tundish, ISIJ International, Vol. 62, No.1, pp 56-63 (2022).

(5) Guangye Xu, Kazuhiko Iwai: Effect of the Anode to Cathode Surface Area Ratio on the Concentration Distribution near the Solid-Liquid Interface, Magnetohydrodynamics, Vol. 58, No.1-2, pp 109-114 (2022).

(6) Guangye Xu, Kazuhiko Iwai: Materials Transactions, under reviewing.

Presentations

Domestic Conference

(1) Guangye Xu, Kazuhiko Iwai: Decrease of concentration boundary layer thickness by imposing magnetic field. Oral presentation at: 66th The Japan Society of Applied Physics (JSAP) Spring Meeting, Tokyo, Japan. March 9-12nd, 2019.

(2) Guangye Xu, Kazuhiko Iwai: Decrease of concentration boundary layer thickness by adding alternating electrical current and magnetic field simultaneously. Oral presentation at: 177th The Iron and Steel Institute of Japan (ISIJ) Meeting, Tokyo, Japan. March 20-22nd, 2019.

(3) Guangye Xu, Kazuhiko Iwai: Concentration boundary layer thickness decrease mechanism analysis under magnetic field imposition through Cu^{2+} concentration time variation. Oral presentation at: 67th JSAP Autumn Meeting, Sapporo, Japan. September 18-21st, 2019.

(4) Guangye Xu, Kazuhiko Iwai: Velocity estimation for concentration boundary layer thickness decrease mechanism analysis under simultaneous imposition of current and magnetic field. Oral presentation at: 178th ISIJ Meeting, Okayama, Japan. September 11-13rd, 2019.

(5) Guangye Xu, Kazuhiko Iwai: Evaluation of liquid velocity near solid-liquid interface under the superimposition of DC current and magnetic field with or without AC current. Oral presentation at: 180th ISIJ Meeting, online. September 16-18th, 2020.

(6) Guangye Xu, Kazuhiko Iwai: Length ratio effect of anode to cathode on concentration boundary layer under time-varying force imposition. Poster presentation at: 2021 ISIJ Hokkaido branch Meeting, online. July 17th, 2021.

(7) Guangye Xu, Kazuhiko Iwai: Effect of micro-scale flow excitation on solute concentration time variation near solid-liquid interface. Oral presentation at: 184th ISIJ Meeting, Fukuoka, Japan. September 21-23rd, 2022.

International Conference

(1) Guangye Xu, Kazuhiko Iwai: Effect of anode to cathode surface area ratio on concentration distribution near solid-liquid interface. Oral presentation at:

Electromagnetic processing of materials (EPM) 2021 conference, Riga, Latvia. June 14-16th, 2021 (online presentation).

Award

2019.03 11th English Presentation Award of the 66th The Japan Society of Applied Physics Spring Meeting